COMBUSTION AND DIRECT ENERGY CONVERSION IN A MICRO-COMBUSTOR

A Thesis

by

YAFENG LEI

Submitted to the Office of Graduate Studies of
Texas A&M University
in partial fulfillment of the requirements for the degree of

MASTER OF SCIENCE

August 2005

Major Subject: Mechanical Engineering

COMBUSTION AND DIRECT ENERGY CONVERSION IN A MICRO-COMBUSTOR

A Thesis

by

YAFENG LEI

Submitted to the Office of Graduate Studies of
Texas A&M University
in partial fulfillment of the requirements for the degree of

MASTER OF SCIENCE

Approved by:

Chair of Committee,	Kalyan Annamalai
Committee Members,	Ali Beskok
	Nguyen P. Hung
Heat of Department,	Dennis O'Neal

August 2005

Major Subject: Mechanical Engineering

ABSTRACT

Combustion and Direct Energy Conversion in a Micro-Combustor. (August 2005)

Yafeng Lei, B.En., Tianjin University

Chair of Advisory Committee: Dr. Kalyan Annamalai

The push toward the miniaturization of electromechanical devices and the resulting need for micro-power generation (milliwatts to watts) with low-weight, long-life devices has led to the recent development of the field of micro-scale combustion. Since batteries have low specific energy (~200 kJ/kg) and liquid hydrocarbon fuels have a very high specific energy (~50000 kJ/kg), a miniaturized power-generating device, even with a relatively inefficient conversion of hydrocarbon fuels to power, would result in increased lifetime and/or reduced weight of an electronic or mechanical system that currently requires batteries for power.

Energy conversion from chemical energy to electrical energy without any moving parts can be achieved by a thermophotovoltaic (TPV) system. The TPV system requires a radiation source which is provided by a micro-combustor. Because of the high surface area to volume ratio for micro-combustor, there is high heat loss (proportional to area) compared to heat generation (proportional to volume). Thus the quenching and flammability problems are more critical in a micro-scale combustor. Hence innovative schemes are required to improve the performance of micro-combustion.

In the current study, a micro-scale counter flow combustor with heat recirculation is adapted to improve the flame stability in combustion modeled for possible application to

a TPV system. The micro-combustor consists of two annular tubes with an inner tube of diameter 3 mm and 30 mm long and an outer tube of 4.2 mm diameter and 30 mm long. The inner tube is supplied with a cold premixed combustible mixture, ignited and burnt. The hot produced gases are then allowed to flow through outer tube which supplies heat to inner tube via convection and conduction. The hot outer tube radiates heat to the TPV system. Methane is selected as the fuel. The model parameters include the following: diameter d , inlet velocity u , equivalence ratio ϕ and heat recirculation efficiency η between the hot outer flow and cold inner flow. The predicted performance results are as followings: the lean flammability limit increased from 7.69% to 7.86% and the quenching diameter decreased from 1.3 mm to 0.9 mm when heat recirculation was employed. The overall energy conversion efficiency of current configuration is about 2.56.

DEDICATION

I dedicate this thesis to my parents. They have loved and supported me unconditionally throughout my life and it is because of their blessing and self-sacrifice that I have derived the strength to make this work possible. Thank you both for everything.

ACKNOWLEDGEMENTS

First of all, I would like to thank Dr. Kalyan Annamalai, my advisor, for being a devoted mentor. Thank you for your wisdom, patience, and guidance through my career at Texas A&M University.

I would like to thank my committee members, Dr. Ali Beskok and Dr. Nguyen P. Hung, for their contributions and helpful advice on my research. Also, I would like to thank Dr. N.K. Anand for very useful course.

Thanks to my wife, Yujin, for her encouragement and motivation. Thanks to Yunfeng to be my brother. You are the best big brother anyone could have.

I would like to thank my friend Dr. Huitao Yang for his tremendous support during my hard time, your help can never be acknowledged enough.

NOMENCLATURE

Dimensional Parameters

A_c cross sectional area (m^2)

C tube perimeter (m)

d tube diameter (mm)

D diffusion coefficient (m^2/s)

dx control volume length (m)

E total energy (kJ)

h_i inlet enthalpy (kJ/kg)

h_e outlet enthalpy (kJ/kg)

h_c lower heating value (kJ/kmole)

h_H heat transfer coefficient ($kw/m^2 \cdot K$)

L tube length (mm)

l_c characteristic length of the device (mm)

$\dot{m}_i$ inlet mass flow rate (kg/S)

$\dot{m}_e$ outlet mass flow rate (kg/S)

p pressure (kPa)

p_c characteristic pressure (kPa)

$\dot{Q}$ heat transfer rate (kw)

t time (s)

t_c characteristic time (s)

T_c characteristic temperature (K)

T gas temperature (K)

T_{out} gas temperature in counter flow (K)

u velocity (m/s)

u_c characteristic velocity (m/s)

$\dot{W}$ work (kw)

$\dot{w}_F'''$ chemical reaction rate (kmole/m^3·s)

$\dot{w}_c'''$ characteristic reaction rate (kmole/m^3·s)

Dimensionless Parameters

D_a Damkohler number, $D_a = \dot{w}_c''' l_c / \rho_c u_c$

Kn Knudsen number, $Kn = \lambda_f / l_c$

Le Lewis number, $Le = \alpha_c / D_c$

p_e Peclet number, $p_e = l_c u_c / \alpha_c$

Re Reynolds number, $\mathrm{Re} = u l_c / \nu$

B_i Biot number, $B_i = h l_c / k$

$\overline{p}$ normalized pressure, $\overline{p} = p / p_c$

$\overline{t}$ normalized time

$\overline{T}$ normalized temperature

$\overline{u}$ normalized velocity

$\bar{\dot{w}}'''$ normalized reaction rate

Greek Symbols

α thermal diffusivity (m^2/s)

μ dynamic viscosity (Pa·s)

ν kinematical viscosity (m^2/s)

ρ fluid density(kg/m^3)

c_P specific heat(kJ/kg·K)

λ thermal conductivity(kw/m·K)

η efficiency

ϕ equivalence ratio

Acronyms

TPV thermophotovoltaic

LFL lean flammability limit

MEMS micro-electromechanical system

TABLE OF CONTENTS

Page

Page

LIST OF FIGURES

Page

Page

LIST OF TABLES

1. INTRODUCTION

The last few years have experienced a growing trend in the miniaturization of mechanical and electromechanical engineering devices as a result of the progress made in micro-fabrication techniques. High-precision fabrication of devices in the centimeter-scale range are being made using micro-fabrication techniques such as electro-discharge machining (EDM), laser beam machining (LBM), or focused ion beam machining (FIBM). Devices in the millimeter-scale range are being fabricated using micro-electromechanical systems (MEMS), rapid prototyping and batch-manufacturing techniques [1].

The interest in producing miniaturized mechanical devices opens exciting new opportunities for combustion, especially in the field of micro-power generation because of the need for power-supply devices with high specific energy (small size, low weight, long duration). Typical portable consumer electronics suffer from short operation cycles between charges or replacement, and their overall weight is essentially due to battery weight. Similarly, other more advanced MEMS-based devices depend on battery systems that occupy significant fractions of both the mass and volume of the entire device. The need to reduce system weight, increase operational lifetimes, and reduce unit cost has resulted in development of the field of micro-power generation, high-specific-energy micro-electromechanical power system.

This thesis follows the style of *Journal of Micromechanics and Microengineering*.

The concept behind this new field is to utilize the high specific energy of liquid hydrocarbon fuels in combustion-driven micro-devices to generate power.

Of all the conventional sources of energy, liquid hydrocarbons have the highest specific energy. Compared with electrochemical cells, liquid hydrocarbons have specific energy of between 35 and 300 times greater than present battery technology. For example, methane has specific energy of 50 MJ/kg of fuel and an alkaline battery at 0.6 MJ/kg.

The potential advantage of using liquid hydrocarbon combustion to produce power is shown graphically in Fig. 1.1 [2].

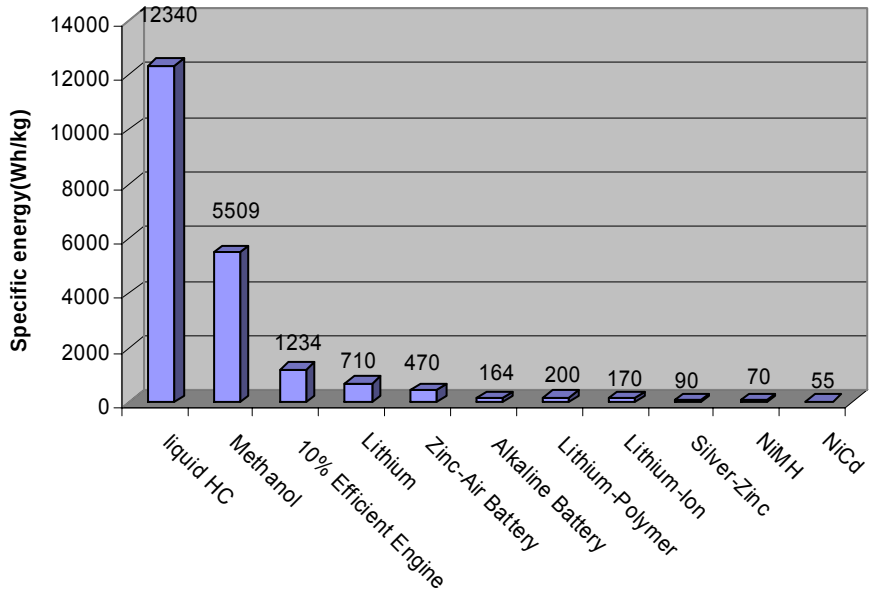

Fig. 1.1 Specific energy for iso-octane and several primary and secondary battery technologies [2].

With such a high specific energy, liquid fuel-based power cells (for applications such as personal electronic devices and remotely located unattended sensors) would be an important enabling technology for a variety of applications. Realization of these power cells will be accomplished by development of micro-engines, micro-combustors combined with an efficient thermal-to-electrical converter (Thermal photovoltaic cell, TPV).

Combustion systems convert chemical energy into thermal energy and have a number of challenges associated with miniaturization:

1) Thermal management
2) Quenching issues

Gas phase combustion will become difficult to achieve except at higher temperatures. Smaller size results in high heat loss and hence quenching becomes an issue. Below certain diameter (or distance between two plates) called quenching diameter (or quenching distance, d_q), flame cannot be sustained. Quenching diameter depends on temperature, pressure and type of fuel used. For hydrocarbon-air combustion at atmospheric pressure and room temperature walls, the quenching diameter is approximate 3 mm. As the reactant temperature is increased at atmospheric pressure, the quenching diameter can be reduced to 1 mm at 600-800 ºC wall temperature. That means high combustion temperature and high wall temperature will overcome the limit of quenching diameter and make combustion possible in micro-scale combustor.

Several methods exist for converting chemical energy to electricity. One of the easiest approaches to producing electrical power from liquid hydrocarbons would be to

integrate a thermoelectric device into a package containing a micro-combustor. Most of the commercial thermoelectric devices are discrete components with a length scale of about 1 mm. The temperature needs for a thermoelectric converter are modest (around 700~900 ºC) and can be easily met. For a TPV system, higher overall efficiency means higher energy density. However, an overall conversion of 5% (limited by the current "ZT factors", the characterization factor that takes into account the electronic and thermal properties of the material) seriously impacts the useful energy density. If high ZT materials are discovered and developed, thermoelectric could become very attractive. Thermal photovoltaic (TPV) could provide higher efficiency around 10%. But it requires high operating temperature of the micro-combustor (exceed 1200 ºC). A demonstrated micro-scale TPV system has not yet been developed.

Currently, there is consensus, at least among those working in the field, that combustion in the micro-scale is possible with proper thermal management. Several meso-scale and micro-scale combustors have been developed that appear to operate with good combustion efficiency. The current study deals with modeling of combustion and flame stability of micro-scale combustor.

2. LITERATURE REVIEW

A literature review is presented in this section. Since micro-technology especially micro-energy system technology is a relatively new field, the literature is very limited. However, several micro-power generation systems are now under development around the world. The achievements showed promising future of the application in the field of micro-combustion. The MIT gas turbine laboratory is developing a MEMS-based gas turbine power generator (Fig. 2.1) with a total volume of approx 300mm^3, designed to produce 10-20 W [3]. It includes a radial compressor/turbine unit, a quartz combustion chamber, and an electrical generator incorporated in the compressor. At the UC Berkeley Combustion Laboratories, a research project is currently underway to develop a liquid hydrocarbon fueled internal combustion rotary engine (Fig. 2.2) [4]. Two engines are currently being developed, one is "mini-rotary engine" designed to delivery power on the order of 30 W. It has a rotor approximately 10 mm in size. The other is "micro-rotary engine" designed to produce power in the milliwatt range. Recently, the rotor size has been reduced to as low as 1 mm [5].

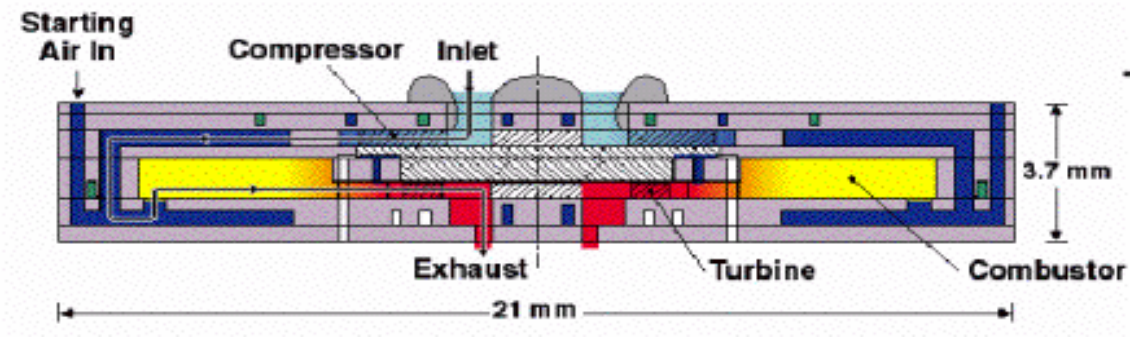

Fig. 2.1 MEMS-based gas turbine [3].

In the design of MEMS-based gas turbine engine, many challenges have been encountered [6]. The low Reynolds number, 10^3~10^5, are simply a reflection of the small size, and place the design in the laminar or transitional range. For example, the values are low enough that it is difficult to force the flow either in a rotor or a stator without separation. The design challenges introduced by the low Reynolds number are exacerbated by geometric restrictions imposed by current micro-fabrication technology. It is well known that high work on the fluid m eans large fluid density change. But the current conventional micro-fabrication technology is not amenable to fabricate variable passage height to accommodate density change. High turbine inlet temperature also requires film cooling to achieve high efficiency and safe working conditions.

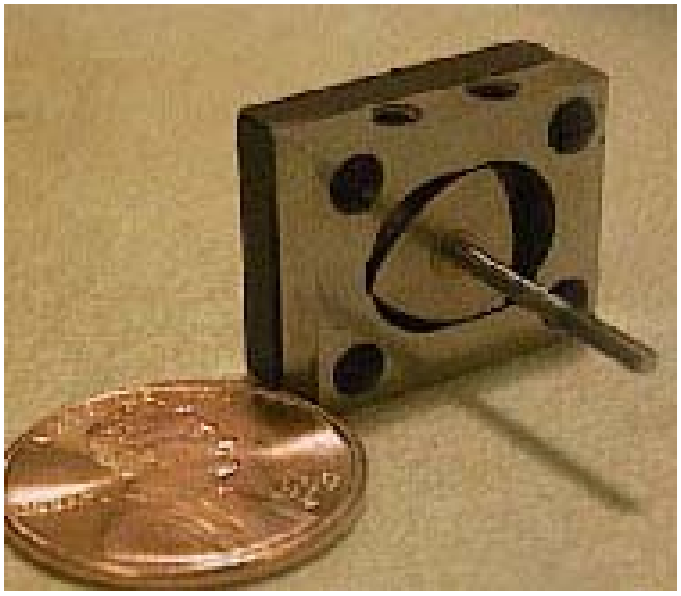

Fig. 2.2 Mini-rotary engine [4].

Berkeley's rotary engine is well suited for the MEMS fabrication because of its planar design of the rotor and housing, reduced number of parts and self-valving operation. The rotor controls the timing of the intake and exhaust, eliminating the need for the complex valve actuating and valve timing system for reciprocating engines. But for a MEMS engine, it operates at a nearly uniform temperature distribution. This introduces potential problems due to auto-ignition of the premixed charge in the intake manifold and expansion of the preheated gases prior to the compression stroke [4].

The gas turbine and rotary engines involve moving parts. Studies of direct energy conversion methods have attracted many attentions recently in order to eliminate moving parts. The micro-TPV system is one of them which use photovoltaic cells to convert thermal radiation energy from the wall which is heated by the gases produced by combustion of fossil fuels into electricity. The system consists of three main parts: a heat source (combustor), a selective emitter and a photovoltaic array [7]. The micro-TPV system requires an input of radiation from high and uniform temperature of the wall of the micro-combustor. Due to the wall length range of several millimeters, this is one of the advantages of micro-combustor with small Biot number.

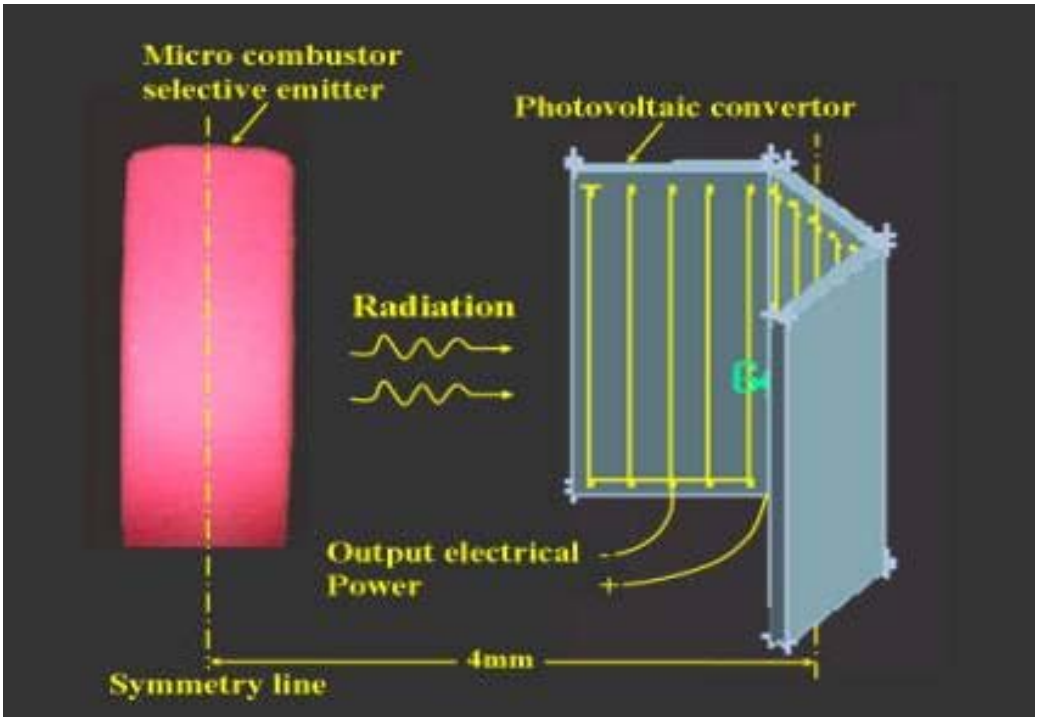

Fig. 2.3 Micro-TPV system [7].

In order to understand the principle of combustion in micro-devices and determine relevant factors affecting micro-combustion, several micro-combustors have been developed. Yang [8][9] fabricated two kinds of stainless steel flame tube combustors, one is straight tube, the other is the straight tube with a sudden expansion step (Fig. 2.4). The tube inner diameter is 2.15 mm. They observed that stable combustion of hydrogen air mixture can only be obtained in straight tube with flow speed at inlet varying from 1.5 to 8 m/s. The Reynolds number varies from 200 to 1000, the turn down ratio of the tube is 5.0. Comparing to straight tube, the other tube with a sudden expansion step can

work steadily under much wider flow rate and wider fuel/air ratio. That's because the flow separation and re-attachment at the expansion step largely enhance the mixing process and prolong the residence time of the fuel mixture, which results in a higher temperature near the wall of combustor. Stable combustion has been obtained with flow speed at inlet varying from 1.5 to 20 m/s and hydrogen/air equivalence ratio varying from 0.45~1.0. An average temperature of about 1300 K along the wall has been achieved with a 12 m/s flow velocity and 0.95 equivalence ratio. While stability is improved due to sudden expansion, it results in a more uneven temperature distribution and induces big thermal stress along the wall.

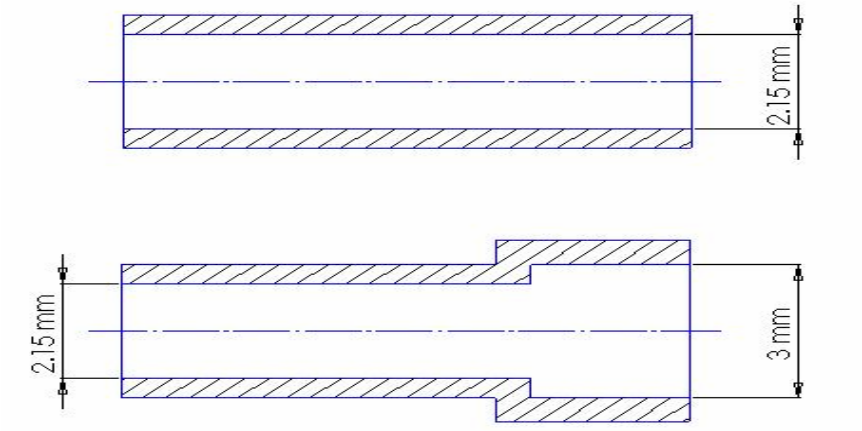

Fig. 2.4 Tube with and without expansion step [8].

As opposed to using sudden expansion step combustor, Sitzki [10] developed spiral counter flow heat-recirculation and catalytic combustion for micro-combustor with channel dimension as low as 0.4 mm (Fig. 2.5). They studied numerically of catalytic combustion in small diameter reactor tubes at low Reynolds numbers to examine its feasibility for MEMS power generator applications using a combination of commercial fluid dynamics code and external subroutines that calculate the surface chemical reactions. They found that Reynolds number as low as 20 can support combustion with heat recirculation and addition of platinum strips as a catalytic material in the combustion region. Catalytic combustion also leads to much lower self-starting temperature.

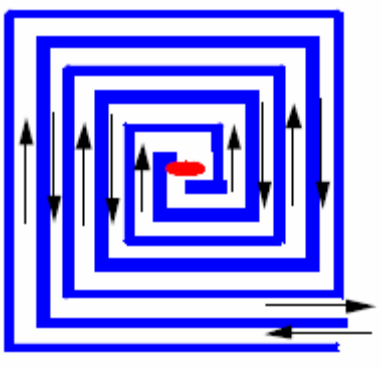

Fig. 2.5 Spiral counter flow combustor [10].

Fu [5] conducted experiments to reduce heat losses from micro-combustors: bundling the tubes together to produce near-adiabatic conditions in the inner tube walls, external heating of the tubes with electrical resistance heating coils, and recirculation of the exhaust gases around the combustor exterior walls. A stable flame was obtained without the use of the electrical heaters in tubes with diameters larger than the quenching diameter. (3.3 mm for CH_4/air at $\phi = 1.0$) However, external heating was necessary in tubes below the quenching diameter. They found that lower power input into the 7-tube bundles is required than the single tube. This means the insulated inner tube require less energy to sustain combustion below the quenching diameter. The external heat flux needed to sustain combustion in the single tubes increased as the tube diameter decreased. They obtained methane-air combustion in quartz tubes with an inner diameter less than 1mm. The authors contend that combustion is still possible on an extremely small scale (0.045 mm) [11] and the limits to combustion on a small scale may come only from the physical material and fabrication limits of the combustion chamber.

The most challenging issue in micro-combustor design of TPV system is to keep an optimal balance between sustaining combustion and maximizing heat output. Sustaining combustion in a micro-combustor is largely affected by the increased heat losses due to the high surface to volume ratio, which tends to suppress ignition and quench the reaction [12]. Furthermore, with the decrease in size, there is less residence time for the mixing (no-premixing combustion) and combustion process, which is critical for achieving stable combustion.

Some of the scaling issues involved in micro-combustion can be understood by normalizing the conservation equations of momentum and energy in terms of the characteristic length and parameters of the device and analyzing their terms as the length scale is reduced. The normalized one dimensional form of the governing equations can be written as: (symbols are defined in the Nomenclature section)

$$\frac{l_c}{t_c u_c}\frac{\partial \overline{u}}{\partial \overline{t}} + \overline{u}\frac{\partial \overline{u}}{\partial \overline{x}} = -\frac{p_c}{\rho_c {u_c}^2}\frac{1}{\overline{\rho}}\frac{\partial \overline{p}}{\partial \overline{x}} + \frac{1}{\mathrm{Re}}\overline{\nu}\frac{\partial^2 \overline{u}}{\partial \overline{x}^2} + \frac{g l_c}{{u_c}^2} \tag{2-1}$$

$$\frac{l_c}{t_c u_c}\frac{\partial \overline{T}}{\partial \overline{t}} + \overline{u}\frac{\partial \overline{T}}{\partial \overline{x}} = \frac{1}{P_e}\overline{\alpha}\frac{\partial^2 \overline{T}}{\partial \overline{x}^2} + D_a \frac{Q}{\overline{c}_p T_c}\overline{\dot{w}'''} \tag{2-2}$$

For a large power system, the Reynolds and Peclet number are also large. Thus the fluid flow are mostly turbulent, and as seen from equation (2-1), (2-2), the viscous and diffusive effects are small compared to the convective effects. It is also deduced that the characteristic time in these convective dominated flows is, $t_c = l_c / u_c$, which is normally referred to as residence time.

For micro-devices with very small characteristic lengths and consequently small Reynolds and Peclet number, the flow is primarily laminar, viscous effects and the diffusive transport of mass and heat become increasingly important. In this case, the residence time decreases but it has to be larger than the chemical time, $t_c = \rho_c / \dot{w}'''$, for complete combustion to occur.

The characteristic length of the micro-combustors being developed to date, even in MEMS size systems, is sufficiently larger than the molecular mean free path of the air and other gases flowing through the systems that the physical-chemical behavior of the

fluids is fundamentally the same as in their macro-scale counterparts. For example, the Knudsen number for air flowing through a 0.1 mm wide channel is of the order of 10^{-3}, which is still smaller than that for free-molecule flow (Kn>0.01). Consequently the standard hypotheses of thermofluids such as the no-slip condition and the continuum medium will still apply. But with the development of MEMS field, the fluid flow in micro-energy systems will be possible in the range of slip regime (0.01<Kn<0.1), the often assumed no-slip boundary conditions seem to fail, Knudsen layer starts to become dominant between the bulk flow and the wall surface. The flow in the Knudsen layer can not be analyzed with the N-S equation and it requires special solutions of the Boltzmann equation. Wall effect should be taken into serious consideration for the system design [13].

One of basic problems in combustion is flame quenching which is to determine the minimum size of a passage such as a tube diameter, orifice size, or distance between plates through which a flame will not propagate. If the flame is to propagate, the energy release due to chemical reaction must keep the reaction zone temperature high enough to sustain a rapid reaction. If heat transfer to the surrounding surfaces is high enough, the temperature will drop and reaction will slow down. As the reaction slows down, the energy release rate is lowered, the temperature drops below the ignition temperature, and the flame will be quenched. Quenching diameter (or distance between tow plates) depends on the geometry of the walls, fuel type, stoichiometry, pressure, reactant temperature, and turbulence. Plots of quenching diameter (distance) versus equivalence ratio are essentially parabolic, with the minimum on the rich side of stoichiometric. On

the lean side, the quenching diameter (distance) is inversely proportional to burning velocity. The quenching diameter (distance) is roughly inversely proportional to pressure. The effect of turbulence is less well known, but increased turbulence should increase the heat transfer and thus increase the size of the quenching diameter (distance). Heating of the wall can also reduce the quenching diameter (distance) by reducing heat transfer. Quenching diameter (distance) for various stoichiometric fuel-air mixture has been given by Bartok and Sarofim. For example, the parallel-plate quenching distance of stoichiometric methane-air mixture at 1 atm and 293 K is 1.9 mm. Note that the quenching distance for parallel plates is 65% less than the circular quenching diameter.

Flammability is a very important character of the flammable gases. The sustaining combustion flame can be ceased by addition of diluent gases in sufficient quantity. Such diluents may consist of excess fuel or excess oxidant or inert gases. The flammability limits can be determined by the quantity of diluents that must be added to a fuel-oxidant mixture to render mixture nonflammable. Bartok and Sarofim give the flammability limits of methane in standard air. The lean limit by volume is 5% and the rich limit is 15%. White gives 5.95% for lean limit and 13.35 for rich limit.

The effect of nonreactive additives such as nitrogen or argon is to reduce the flame temperature and the laminar burning velocity. They also have influence on fuel flammability. Increase the amount of added inert to flammable mixture will narrow the fuel flammability.

The effect of fuel concentration on the laminar burning velocity is shown in Fig. 2.6 [14]. It is seen that laminar velocity for a particular fuel varies by fuel-air ratio.

Hydrogen has the highest burning velocity while methane has the lowest burning velocity. The maximum burning velocities are found just to the rich side of stoichiometric. Fig. 2.7 also illustrates the methane burning velocity [15].

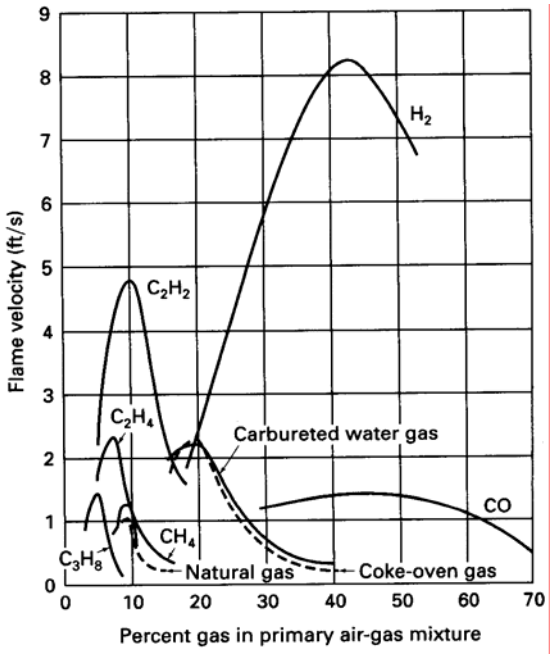

Fig. 2.6 Variation of laminar burning velocity in fuel-air mixtures with variation of fuel content at atmospheric pressure [14].

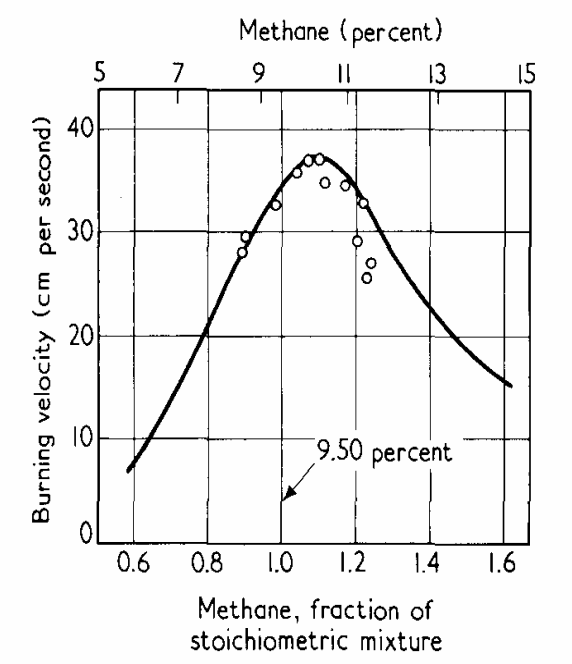

Fig. 2.7 Burning velocities of methane-air mixtures [15].

For slow-burning mixture (burning velocity less than 0.6 m/s), the burning velocity decreases with increasing pressure. For fast-burning mixtures (burning velocity bigger than 0.6 m/s), the burning velocity won't or just slight increase with increasing pressure. The burning velocity increases with the temperature of the reactants. The temperature dependence can be expressed as a power law, and the burning velocity increases as the second or third power of the reactant temperature. Reactant temperature and pressure influence the flammability limits also. Increasing reactant temperature extends the lean limit, but the lean limits are affected only slightly by pressure, whereas the rich limit is extended significantly when the pressure is increased.

The micro-combustor is the most important part in a micro-TPV system. How to get a small and efficient micro-combustor is very critical to the system. In actual applications, there are still some other factors that will influence TPV energy conversion efficiency. It is reported from NASA Glenn Research Center that the overall thermal-to-electric conversion efficiency of TPV system has typically been lower than predicted, primarily because the broadband output of the thermal source does not match the spectral response of those TPV cells that were available. The most popularly used TPV cells are gallium antimony (GaSb). Recent developments in materials and techniques for shaping the output spectrum of a thermal source, and the ability to fabricate TPV cells with tailored spectral response have changed the situation dramatically. Several rare earth oxides, for example, have been shown to have altered spectral distribution in their emission spectra. The radiation changes from its normal broad band to a narrow line superimposed on a low intensity background. Rare earth oxides used this way are called selective emitters which are commonly used in the TPV system design.

The present study explores the feasibility of methane/air combustion in micro-combustor (straight tube combustor) but with heat recirculation. The study will also investigate the application of micro-combustion to TPV system as well as overall energy conversion efficiency.

3. OBJECTIVE

The overall objective of the current study is to explore the possibility of thermo photovoltaic power generation using micro-combustors.

In order to achieve the overall objectives the following tasks must be carried out:

1. Develop a counter flow system for stable combustion and model the combustion of gaseous fuel in a micro-tube.
2. Include simplified radiation model for a thermal photovoltaic system.
3. Determine overall energy conversion efficiency.
4. Conduct parametric studies.

Section 4 presents a description of modeling and numerical procedure while section 5 presents results and discussion.

4. THEORETICAL FORMULATION OF THE MICRO-COMBUSTION MODEL

This section presents a combustion model for the micro-combustor with heat recirculation.

4.1 Assumption and simplification of the combustion model

Fig. 4.1 is the physical model of micro-combustor selected for the current study. This model includes a combustion tube with inner diameter varying from 1~3 mm and an annular outer tube which serves as a counter flow heat exchanger. The outflow diameter is selected such that cross sectional areas are set to be equal. For a micro size combustor, the reduced diffusion time due to small size has a crucial effect on the rapid uniformity of concentration distributions near a flame in the combustor. In addition, the flow is laminar, which prevents the achievement of rapid mixing between fuel and air due to the low transport coefficients related to mass and heat transfer in combustor. Therefore, premixed combustion instead of diffusion combustion should be selected in micro-combustor. The flame propagation in the current model is two-dimensional in nature. However, if we limit our interest to micro-scale burners with tube diameter and wall thickness much smaller compared with the tube length scale, we can simplify the problem to be one-dimensional. Thus the one dimensional plug laminar flow assumption is applied to this model. Radiation heat transfer between gases and walls is negligible compared to convective heat transfer.

The pressure drop of the gas flow in the tube ΔP has been roughly calculated [16] for the base case where the inlet speed is 1 m/s and inner diameter is 3 mm:

$$\triangle p = (f\frac{L}{D} + k)\frac{\rho v^2}{2}$$

For the base casa, the friction factor f=64/Re=64/200=0.32 , L/D=60/3=20 , the loss coefficient $k = 1.5$, $\rho = 1.13 kg/m^3$, so the pressure drop is around 4.46 kPa . The pressure drop in the tube has been neglected for the current model.

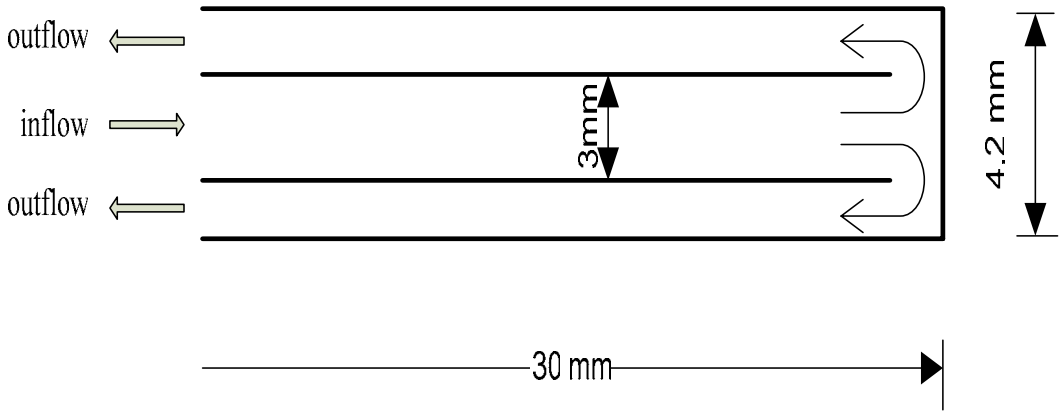

Fig. 4.1 Micro-combustor in the theoretical model (carbon steel)

4.2 Heat transfer issues in the combustion model

The order of magnitude of the heat transfer within the tubes and between the tube and the surrounding air can be obtained with a simple one-dimensional, steady state calculation. In the present model, the heat transfer is expressed in a convective form where the amount of heat transfer is determined by the empirical heat transfer coefficient. A more realistic expression of heat transfer should include the convection within the combustor, the conduction through the combustor wall, convection on both sides of the inner tube wall surfaces and heat transfer through outer tube including outer surface radiation. Fig. 4.2 schematically displays heat transfer modes of the micro-tube. Fig. 4.3 presents the thermal resistance concept for the micro-combustor. The wall temperatures are denoted by $T_{w,1}$, $T_{w,2}$, $T_{w,3}$ and $T_{w,4}$ for the outer and inner tubes while T_g represents gas temperature for the inner tube, $T_{g,o}$ represents gas temperature in the outer tube. Fig. 4.3 presumes that wall thicknesses are small.

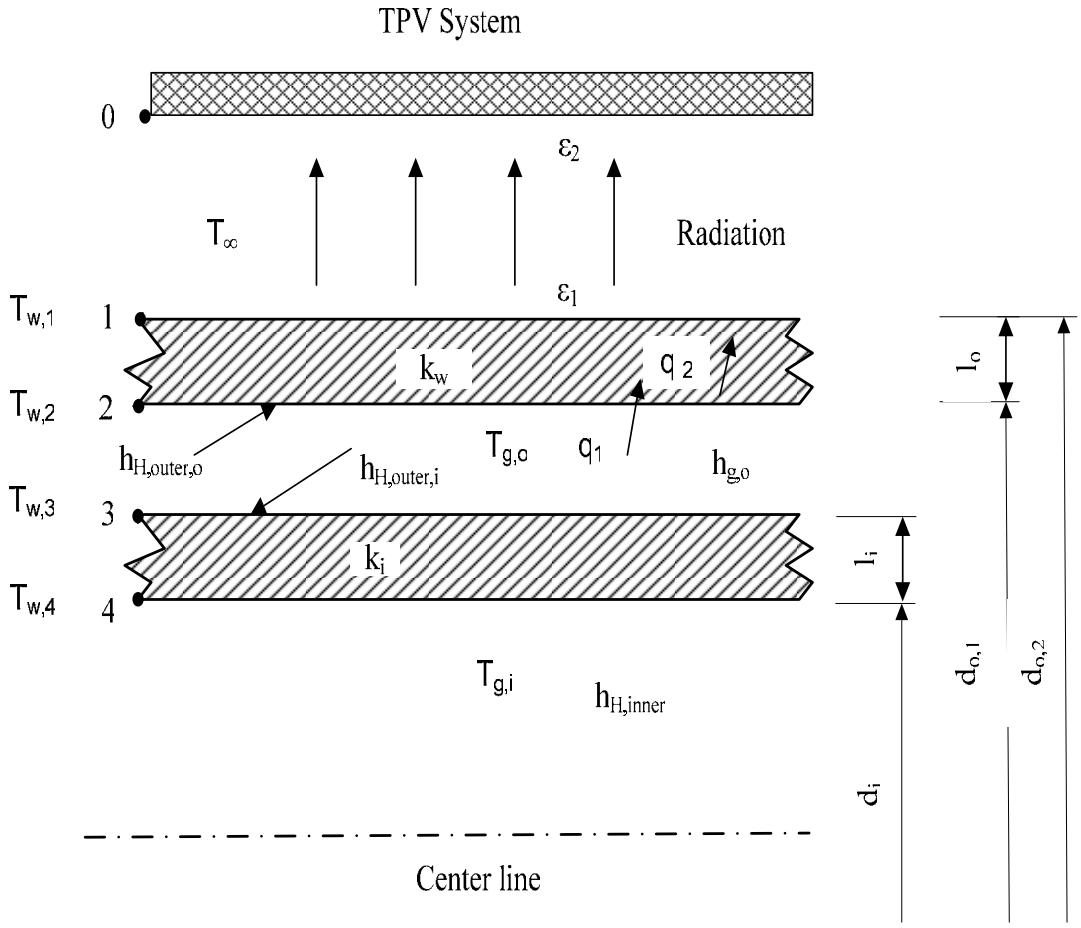

Fig. 4.2 Heat transfer mode in micro-combustor

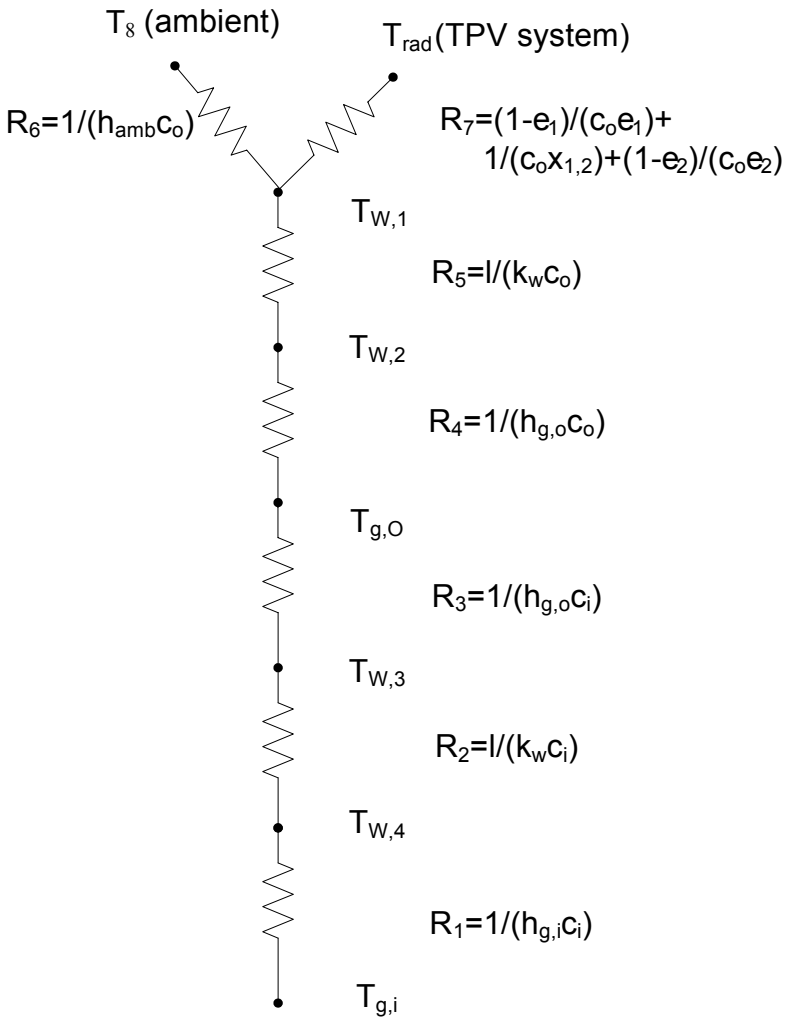

Fig. 4.3 Thermal resistance concept for the micro-combustor of unit length

4.2.1 Convective heat transfer correlation

Let q_1' be the convective heat transfer per unit length of inner wall of outer tube and q_2' the conduction heat transfer through the combustion wall.

The heat fluxes are given by:

$$q_1' = h_{g,o}(T_{g,o} - T_{w,2})\pi d_{o,2} \quad \text{, w/m} \tag{4-1}$$

$$q_2' = \frac{k_w}{l_o}(T_{w,2} - T_{w,1})\pi d_{o,2} \quad \text{, w/m} \tag{4-2}$$

Combining equation (4-1) and (4-2) with $q_1 = q_2$ under steady state, the following relation can be obtained:

$$\frac{h_{g,o} l_o}{k_w} = -\frac{T_{w,2} - T_{w,1}}{T_{g,o} - T_{w,2}} \tag{4-3}$$

Recall that

$$Nu_o = h_{g,o} d_{o,2} / k_{g,o}$$

Equation (4-3) becomes:

$$\frac{h_{g,o} l_o}{k_w} = Nu_o \frac{k_{g,o}}{k_w} \frac{l_o}{d_{o,2}}$$

where,

$$Nu_o \frac{k_g}{k_w} \frac{l_o}{d_2} = -\frac{T_{w,2} - T_{w,1}}{T_{g,o} - T_{w,2}}$$

$$Nu_o = f\left(\frac{T_w}{T_{g,o}}, \frac{k_w}{k_g}, \frac{d}{l}\right) \tag{4-4}$$

Expressing (4-4) explicitly shows the dependence of the heat transfer on the temperatures (T_w/T_g), the material and gas properties (kw/kg), and the geometric shapes (d/l) of the combustor.

In this model, to be simple, Nu of the inner tube is determined by the empirical correlation [17] using constant wall temperature as following:

$$Nu = \frac{h_{inner} d_i}{k} = \frac{4.364 + Bi}{1 + 0.2682 Bi} \tag{4-5}$$

where Bi is the Biot number of the micro-tube. This dimensionless Biot number reflects the effect of the wall thermal resistance. This empirical correlation is applicable to the forced convection of laminar flow in circular duct. The Biot number is 0.14 for quartz tube and 0.006 for steel in current micro-scale. As Biot number decrease to zero, then from equation (4-5), Nusselt number will reach 4.364.

For the outer tube, heat transfer occurs to the outer wall of inner tube with a heat transfer coefficient of $h_{outer,i}$. Further, heat loss occurs via radiation from outer wall of outer tube. Thus, one needs another heat transfer coefficient $h_{outer,o}$ for outer wall. Heat transfer literature use hydraulic diameter for annular tube, $d_h = d_o - d_i$ and presents $Nu_{outer,i}$ and $Nu_{outer,o}$ correlations for limited wall conditions. $Nu_{outer,i}$ is 5.38 and $Nu_{outer,o}$ is 4.602 [18]. For simple, the Nusselt number of both inner and outer tube is defined as 4.364, which means $h_{H,outer,o} = h_{H,outer,i} = h_{H,outer} = h_{H,inner}$.

4.2.2 Radiation heat transfer

If one neglects natural convection of the outer tube compared to radiation heat loss, the convective heat transfer between the gas in the outer tube and the outer tube wall should be equal to the heat radiation from outer tube wall

to the surrounding:

$$h_{g,o}(T_{g,o} - T_{w,2})d_2 = \frac{k_w(T_{w,2} - T_{w,1})}{l_o} d_2 = [\varepsilon\sigma(T_{w,1}^4 - T_\infty^4)]d_2 \qquad (4\text{-}6)$$

where it is assumed that, $d_2 \approx d_1$, ε is emisivity and σ is Stefan-Boltzmann constant, T_∞ is ambient temperature. Heat loss from micro-tube outer surface towards the ambient will take a large fraction of the total energy input. As the gas gets cooled along the outer tube, less heat is available for transfer to the inner tube containing cold combustible mixture. Smaller combustor size will cause a larger heat loss which would reduce the fuel/air mixture temperature and chemical reaction time.

The chemical reaction time can be expressed as the following:

$$\tau_{che} \approx \frac{[fuel]_0}{A[fuel]^a[o_2]^b e^{-E_a/(RT)}}$$

$[fuel]_0$ is initial fuel concentration, E_a is the activation energy while *A, a,* and *b* are empirically determined factors.

Residence time is given as:

$$\tau_{res} = \frac{L}{u}$$

where, L is tube length and u is gas velocity in the tube.

In order that combustion is complete, $\tau_{che} >> \tau_{res}$.

Since in general the residence time will be less in micro-combustors, it's important to have shorter chemical time to ensure completion of the combustion process within the combustor. Also, reducing the chemical reaction time is the only mean of ensuring complete combustion without compromising the high power density. Chemical time can be reduced by preheating the incoming mixture in the inner tube. This is achieved by transferring heat from hot outer annular tube to the inner tube. The next section presents such a model.

4.3 Combustion modeling

4.3.1 Assumptions

Fig. 4.1 shows the geometry of the counter flow micro-combustor. The combustion is modeled with the following assumptions:

a) One dimensional
b) Negligible heat transfer between gas and wall via radiation
c) Density is only a function of temperature
d) Pressure loss is negligible
e) Gas temperature gradient in the radial direction is zero, any radial heat transfer is accounted through heat transfer coefficient.
f) Le=1
g) Global chemical kinetics
h) For fuel and oxygen conservation equations, diffusion terms are neglected.

Methane is used as fuel in the current model.

4.3.2 Species conservation equation

Using assumption (g), the following relation [14] is adopted for methane consumption rate:

$$\dot{w}_F''' = -AT^n P^m \exp(-\frac{E}{RT})[CH_4]^a[O_2]^b$$

Fuel and oxygen conservation equations are established as following:

$$\rho u \frac{dy_F}{dx} = \rho D \frac{d^2 y_F}{dx^2} + \dot{w}_F''' \quad \text{(a)}$$

$$\rho u \frac{dy_{O_2}}{dx} = \rho D \frac{d^2 y_{O_2}}{dx^2} + \dot{w}_{O_2}''' \quad \text{(b)}$$

where, y_F is fuel mass fraction and y_{O_2} is oxygen mass fraction in the mixture.

At x=0, $y_F = y_{F.0}$, $y_{o_2} = y_{o_2.0}$, $T = T_0$.

Equation (a) and (b) can be combined and written in term of Schvab-Zeldovich variable as:

$$\rho u \frac{d\beta}{dx} = \rho D \frac{d^2 \beta}{dx^2} \quad \text{(c)}$$

where $\beta = \beta_{o_2 - F} = y_F - \frac{y_{o_2}}{\nu_{o_2}}$, $\nu_{o_2} = \frac{2kmole\ O_2}{kmole\ CH_4}$

4.3.3 Combustion modeling of the inner tube

Based on the assumptions listed from (a) to (t), the fluid flow field has been divided to infinite small control volumes (Fig. 4.4) and the first law of thermodynamics has been applied to each control volume:

$$\frac{dE}{dt} = \dot{Q} - \dot{W} + \sum \dot{m}_i h_{tot,i} - \sum \dot{m}_e h_{tot,e}$$

where $h_{tot} = h_f + h$ is total enthalpy, h_f is enthalpy of formation, h is thermal enthalpy.

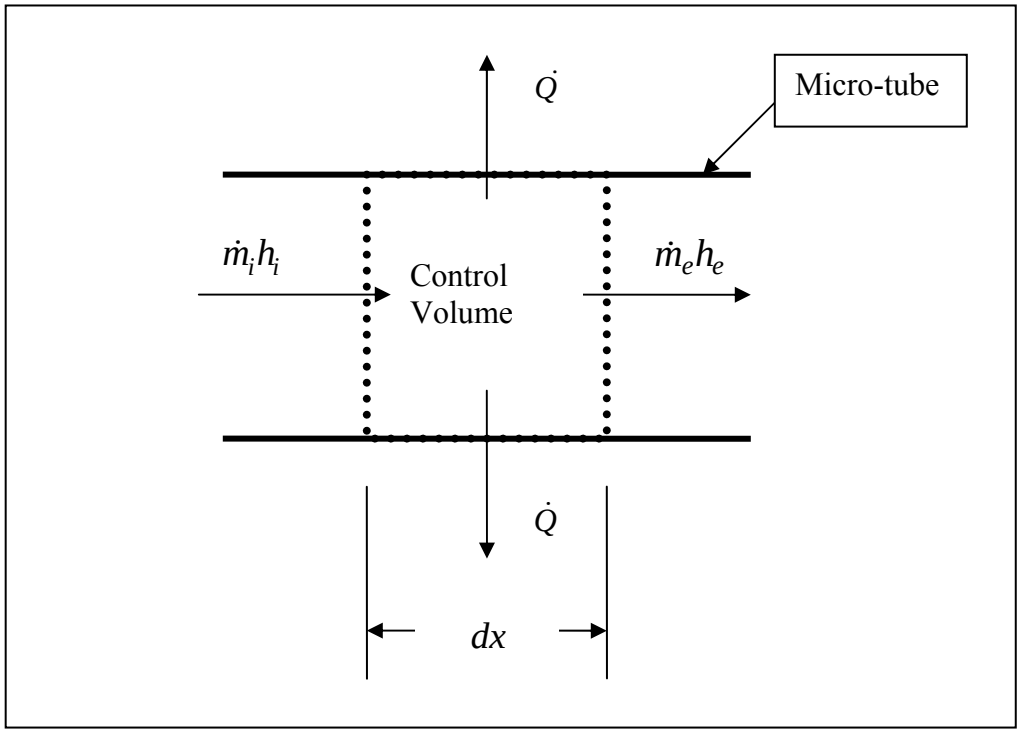

Fig. 4.4 Heat balance in the control volume

So, $$\frac{dE}{dt} = \dot{Q} - \dot{W} + \sum \dot{m}_i h_i - \sum \dot{m}_e h_e + \left|\dot{w}_F'''\right| h_c A_i dx \tag{4-6}$$

where $$\dot{Q} = \dot{Q}_p + \dot{Q}_{cs,in} - \dot{Q}_{cs,out}$$

$$\dot{Q}_p = h_H C_i dx (T_{g,o} - T)$$

$$\dot{Q}_{cs,in} = -\lambda \frac{dT}{dx} A_i$$

$$\dot{Q}_{cs,out} = -\frac{d}{dx}(\lambda \frac{dT}{dx} A_i) dx - \lambda \frac{dT}{dx} A_i$$

where, $h_H = 1/(1/h_{H,outer} + l_i / k_i + 1/h_{H,inner})$ is heat transfer coefficient between gas in inner and outer tube, $T_{g,o}$ is local gas temperature in outer tube, $T = T_{g,i}$ is local gas temperature in the inner tube, h_c is heat value per unit mass of fuel, $\dot{w}_F'''$ is chemical reaction rate, $\dot{Q}_p$ is heat flux from the outer tube to inner tube via convection, $\dot{Q}_{cs,in}$ is heat flux into the control volume via conduction and $\dot{Q}_{cs,out}$ is heat flux out the control volume via conduction. A_i is inner tube cross section area, C_i is circumference of inner tube.

For steady state condition without any work transfer, equation (4-6) can be rewritten as the following:

$$0 = h_H C_i dx (T_{g,o} - T) + \left|w_F'''\right| h_c A_i dx + [\rho u c_p A_i T + (-\lambda A_i \frac{dT}{dx})] -$$
$$[\rho u c_p A_i T + \frac{d}{dx}(\rho u c_p A_i T) dx + (-\lambda A_i \frac{dT}{dx}) + \frac{d}{dx}(-\lambda A_i \frac{dT}{dx}) dx]$$

The energy balance equation for the inner tube is written as:

$$\rho u c_p A_i \frac{dT}{dx} = \lambda A_i \frac{d^2T}{dx^2} + h_H C_i (T_{g,o} - T) + \left|\dot{w}_F'''\right| h_c A_i \tag{4-7}$$

Combining Equation (a) and (4-7), we get:

$$\rho u \frac{d\beta}{dx} = \rho D \frac{d^2\beta}{dx^2} + \frac{h_H C_i}{h_c A_i} (T_{g,o} - T) \tag{4-7'}$$

where $$\beta = \beta_{h_t - F} = \frac{h_t}{h_c} + y_F, \quad h_t = c_p T$$

Because of radial heat transfer between inner and outer tube, $\beta_{h_t - F} \neq \beta_{o_2 - F}$.

4.3.4 Combustion modeling of the outer tube

For the outer tube, we can get a similar expression:

$$\rho u c_p A_o \frac{dT}{dx} = \lambda A_o \frac{d^2T}{dx^2} + h_H C_i (T_{g,i} - T) + h_{H,outer,o} C_o (T_{w,1} - T) + \left|\dot{w}_F'''\right| h_c A_o \tag{4-8}$$

where, $T = T_{g,o}$, $h_{H,outer,o}$ is heat transfer coefficient between gas and outer tube.

The wall temperature of outer tube T_{wall} can be calculated using equation (4-5).

4.3.5 Discretization of energy differential equations

According to different fuel inlet conditions, we pick an adequate discretization scheme such as up-wind scheme [19][20] to calculate the temperature distribution along the micro-combustor. Mass flow rate is constant in the combustor, the velocity of fluid flow is assumed to be only a function of temperature.

For example, Fig. 4.5 illustrates three successive control volumes n-1, n, n+1.

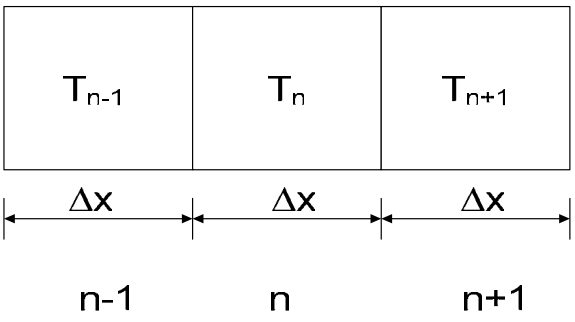

Fig. 4.5 Successive control volumes

By integrating equation (4-7) over the control volume n, we can get:

$$\rho u c_p A_i (T_n - T_{n-1}) = \lambda A_i \left[\frac{(T_{n+1} - T_n)}{\Delta x} - \frac{(T_n - T_{n-1})}{\Delta x} \right] + h_H C_i (T_{g,o} - T)\Delta x + \left| \dot{w}_F''' \right| h_c A_i \Delta x$$

Rewriting the equation, we obtain:

$$a_p T_n = a_w T_{n-1} + a_e T_{n+1} + s\Delta x \tag{4-9}$$

where,

$$a_p = \rho u c_p A_i + \frac{2\lambda A_i}{\Delta x} + h_H C_i \Delta x$$

$$a_w = \rho u c_p A_i + \frac{\lambda A_i}{\Delta x}$$

$$a_e = \frac{\lambda A_i}{\Delta x}$$

$$s = h_H C_i T_{g,o} + \left| \dot{w}_F''' \right| h_c A_i$$

The inlet boundary condition is defined as the inlet mixture temperature which is the ambient temperature and the outlet boundary condition is defined as the zero

temperature gradient. Using the inlet and outlet boundary conditions, we can solve the equation (4-7) and (4-8) by iteration.

4.3.6 Numerical procedure

The numerical calculation procedure is as following:

1) Assume initial gas temperature to be 300 K except ignition cell I where the temperature T_I is ignition temperature and the ignition begins in this cell. At x=0, the inlet temperature is always set to be 300 K.
2) Start reaction at cell I with $y_F = y_{F,0}$, $y_{o_2} = y_{o_2,0}$.
3) Determine $\left|\dot{w}_F'''\right|$ in each cell. By ignoring diffusion terms, change in y_F along the tube is calculated, then we get new y_F and y_{o_2} values.
4) Use discrete energy differential equations (4-9) and get new gas temperature. Use the following heat transfer equations to calculate wall temperature:

$$h_{g,o}(T_{g,o} - T_{w,1}) = \varepsilon \sigma (T_{w,1}^4 - T_\infty^4)$$

where it is assumed that there is negligible resistance within the wall material.

5) Repeat step 1 to 4 until convergence occurred.

Appendix C illustrates the iteration procedure of the combustion simulation from initial condition to steady state for the base case.

4.4 TPV system modeling

The black body hemispherical spectral emissive power is given by Planck's radiation law (Fig. 4.6).

$$E_{b\lambda} = \frac{C_1 \lambda^{-5}}{e^{C_2/(\lambda T)} - 1} \qquad \text{W/m}^3$$

where, $C_1 = 3.742 \times 10^{-16} W \cdot m^2, C_2 = 1.4388 \times 10^{-2} m \cdot K$

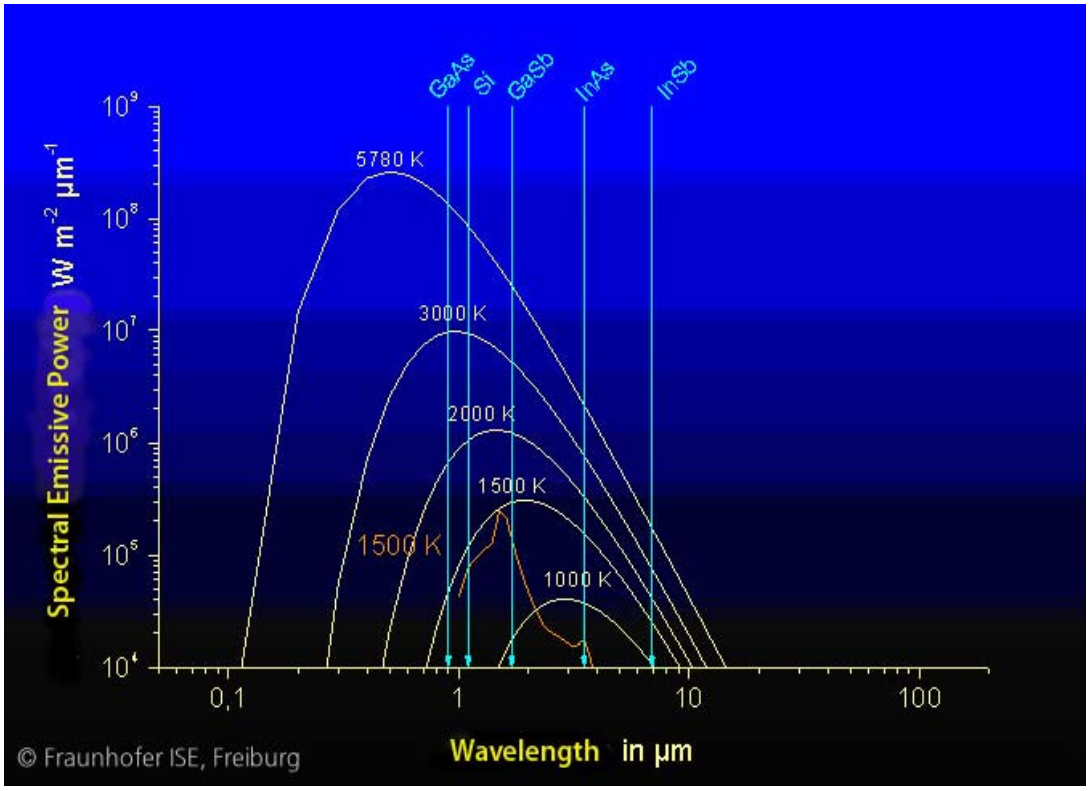

Fig. 4.6 TPV cells' spectrum absorption range

Fig. 2.3 illustrates a typical TPV system using a combustion source. Using calculated wall temperature along the outer wall of outer tube ($T_{w,1} = T_{w,1}(x)$), the spectrum emissivity can be determined. It is seen that the spectral output shifts to large wave length at lower $T_{w,1}$.

The range of spectrum within which the photon energy can be converted into electricity depends on the type of TPV cells. Fig 4.6 shows the ranges of spectrums for various TPV systems. For the current modeling study, the GaSb (gallium antimony) cells are used as a photovoltaic converter which has a band gap of 0.72 eV. This implies that photons from heat radiation with a wavelength smaller than 1.7 μm can only produce electricity on the GaSb cells.

5. RESULTS AND DISCUSSION

This section presents the results for combustion performance of micro-combustor when it is fired with methane, temperature profiles along inner and outer tubes, and finally the degree of conversion of thermal energy into electrical energy. A computer code has been developed to determine the micro-combustor performance.

5.1 Data used in combustion code

Table 5.1 lists the geometrical data, fuel and transport properties, operational parameters, chemical kinetics and other data used in the combustion code for the base case.

Table 5.1: Base case data

GEOMETRICAL DATA		
Diameter of inner tube, d_i	3	mm
Diameter of outer tube, d_o	4.2	mm
Tube length, L	30	mm
OPERATIONAL PARAMETERS		
Inlet velocity, u	1	m/s
Inlet temperature of mixture, T_i	300	K
Ambient pressure, p	1	Bar
Ambient temperature, T_∞	300	K

Table 5.1: Continued

FUEL PROPERTIES		
Fuel	CH4	
Lower heating value, h_c	800000	kJ/kmole
TRANSPORT PROPERTIES OF FUEL/AIR MIXTURE		
Specific heat, c_p	1.4	kJ/kg K
Gas conductivity, k	0.0763	W/m K
Viscosity, μ	17×10^{-6}	kg/m s
Pr	0.56	
DATA OF GLOBAL CHEMICAL KINETICS		
A	1.3×10^{9}	
E	202408	kJ/kmole
a	0.3	
b	1.3	
n	0	
m	0	
OTHER DATA		
Equivalence ratio	0.83	
Emissivity of outer tube	0.93	
Effective wavelength	< 1.7	μm
TPV cell	GaSb	
TPV cell length	30	mm
Mole weight of mixture	28	kg/kmole

Except the base case, combustions have been studied under variable cases listed in Table 5.2:

Table 5.2: Parametric studies

Inlet velocity, u	m/s	0.5~3
Equivalence ratio, ϕ		0.4~1.2
Inner diameter, d_i	mm	0.5~ 5
Heat transfer coefficient, h_H	w/m^2k	50~200

All the parameters and thermal resistances in Fig. 4.3 present in Table 5.3:

Table 5.3: Data used in the thermal concept analysis

Nusselt number of inner tube, Nu_i		4.364
Nusselt number of the outer surface of inner tube, $Nu_{outer,i}$		5.38
Nusselt number of the inner surface of outer tube, $Nu_{outer,o}$		4.602
Inner heat transfer coefficient, $h_{H,inner}$	w/m^2·K	111
Heat transfer coefficient of the outer surface of inner tube, $h_{H,outer,i}$	w/m^2·K	342
Heat transfer coefficient of the inner surface of outer tube, $h_{H,outer,o}$	w/m^2·K	292
Wall thickness, l	mm	≈ 0
Perimeter of inner tube, c_3 or c_4	mm	9.42
Perimeter of outer tube, c_1 or c_2	mm	13.2
Thermal resistance, R_1	k/w	0.956
Thermal resistance, R_2	k/w	≈ 0
Thermal resistance, R_3	k/w	0.222
Thermal resistance, R_4	k/w	0.259
Thermal resistance, R_5	k/w	≈ 0
Thermal resistance, R_6	k/w	≈ 0

5.2 Flame structure and temperature distribution

In the base case study, the Peclet number is set to 4, which means the grid size is 0.2 mm and the amount of node is 150 for 30 mm length tube. At this grid size the results will keep unaffected even increasing the node amount.

In order to get the steady temperature distribution, the initial temperature profile for iteration #1 assumes high temperature within a small region in the inner tube so that chemical heat release is significant enough to cause ignition and combustion. Once it occurs, heat diffuses around the intensive reaction regime causing a new temperature distribution for iteration #2. Temperature profiles for iteration #2 are compared with temperature profiles for iteration #1 and iterations continue until successive profiles are similar.

Using the numerical solution procedure outlined in section 4 and the base case data presented in previous section, performance results were obtained for the base case. Figure 5.1 presents the gas temperature profile in the inner and outer tube, and mass fraction of fuel and oxygen in the inner tube.

At the location of x=14.5mm, the gas has been heated to around 650 K due to radiation heat transfer from outer tube and heat conduction from the reaction zone. The preheating causes the reaction rate to increase rapidly and the temperature eventually raise to 2300 K at x=15mm along the inner tube.

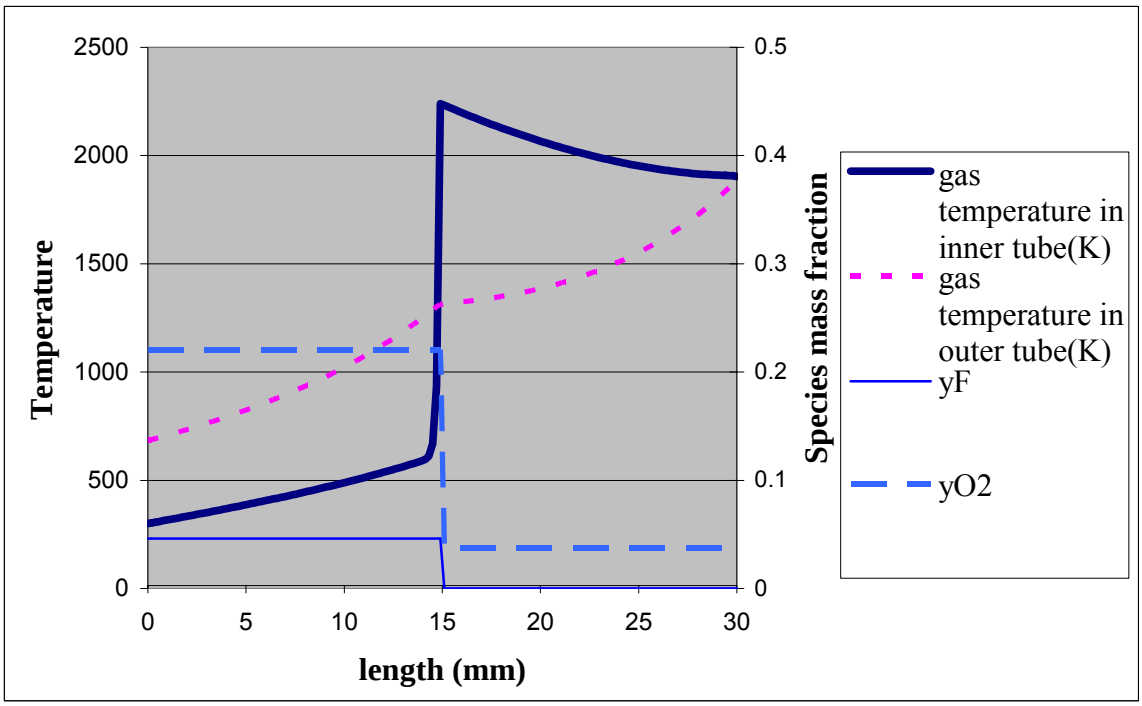

Fig. 5.1 Flame structure and species distribution in the tube

The fuel mass fraction (Y_F) and oxygen mass fraction (Y_{O2}) profiles remain almost flat before the ignition location due to low reaction rate. Once ignited the mass fractions decrease rapidly within the flame zone.

For a tube with 3 mm inner diameter, Figure 5.2 shows the influence of mixture inlet velocity on the flame structure. The combustions are still stable although the mixture inlet velocity is much higher than the stoichiometric laminar burn velocity (40~50 cm/s).

That's because the heat recirculation preheats the cool inlet mixture then cause the combustion to occur.

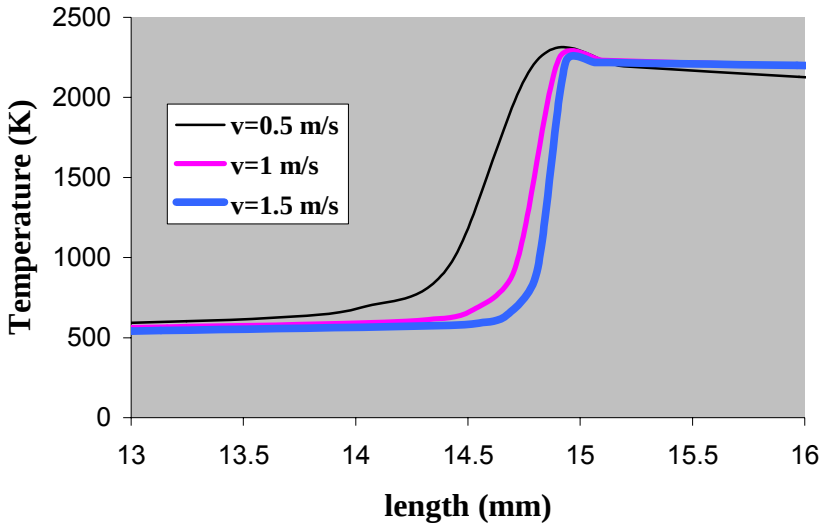

Fig. 5.2 Influence of inlet velocity

Figure 5.3 illustrates the outer wall temperature distribution. The wall temperature for the outer annual tube is lower compared to gas temperature due to heat loss via radiation to TPV system. The discontinuity of the temperature profile is apparently due to intensive combustion occurring in the inner tube.

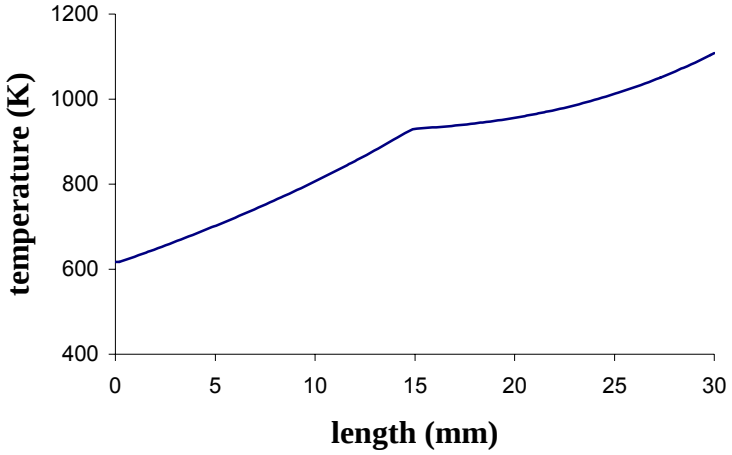

Fig. 5.3 Outer wall temperature

5.3 Flammability limits of micro-combustor

Once ignition is achieved, the next requirement is that combustion is sustained at different air fuel ratios, velocities and diameters. The leanest and richest concentrations, which will just self-support a flame, are called the lean and rich flammability limit respectively. Essentially what determines the flammability limit is a competition between the rate of heat generation, which is controlled by the rate of reaction and the heat of reaction for the limit mixture rates, and the external rate of heat loss from the flame.

Representative flammability limits for various fuels in air are given in Table 5.4. Methane is flammable when the fuel volume percentage is increased from 5 to 15% when cold air/CH4 mixture is supplied.. In view of the accelerating effect of temperature

on chemical reactions, it is reasonable to expect that limits of flammability should be broadened if mixture in the inner tube is preheated using heat from the outer tube.

When the equivalence ratio decreases from base case value of 0.83 to a value called lean flammability limit (LFL), the flame can not be stabilized.

Fig.5.4 shows the lean flammability limit of micro-combustor with and without heat recirculation. Rich flammability limit was not obtained in this section because at fuel rich condition, the combustion will be incomplete.

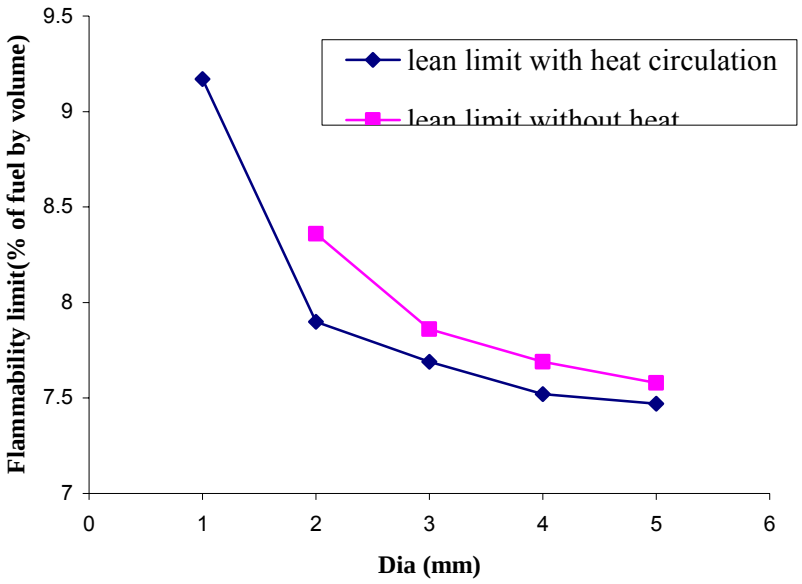

Fig. 5.4 Lean limit of flammability in air (% of fuel by volume)

Fig. 5.5 illustrates the variation of flammability limit with inlet velocity. When heat is transferred from outer to inner tube, mixture can be burned even at mean flow velocities 4 times the stoichiometric laminar burn velocity (40~50 cm/s). The high velocity extinction limit is almost certainly due to insufficient residence time compared to the chemical reaction time scale.

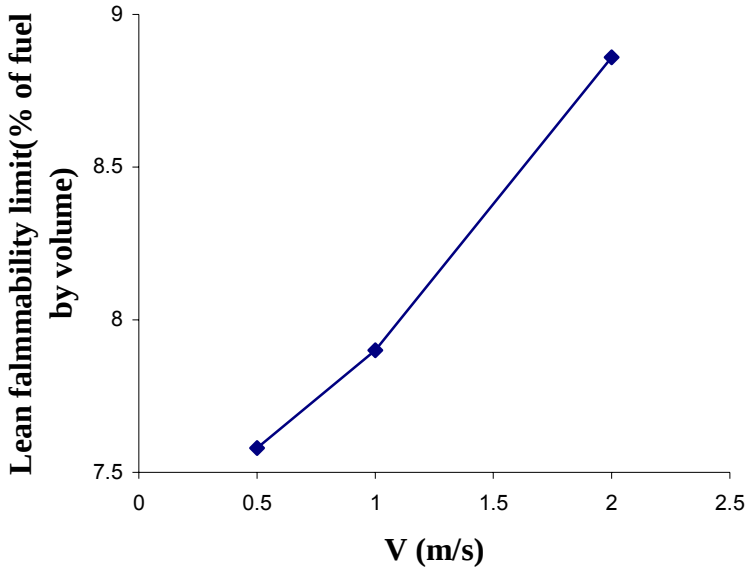

Fig. 5.5 Maximum inlet speed at lean flammability limit

Table 5.4: Flammability limits of some fuels in standard air *(volume percent) [21]

Fuel	**Stoichiometric % volume**	**Lean limit % volume**	**Rich limit % volume**
Methane	9.47	5.0	15.0
Ethane	5.64	2.9	13.0
Propane	4.02	2.0	9.5
Isooctane	1.65	0.95	6.0
Carbon monoxide	29.5	12.5	74
Acetylene	7.72	2.5	80
Hydrogen	29.50	4.0	75
Methanol	12.24	6.7	36

* These flammability properties are dependent on the purity of the substances and on the method of determination used.

5.4 Quenching diameter

The fundamental time constraint can be quantified in terms of a homogeneous Damkohler number, the ratio of the residence time to the characteristic chemical reaction time:

$$Da_h = \tau_{residence} / \tau_{chemical}$$

In order to maintain stable combustion in the tube, the residence time should be longer than the chemical time or the Damkohler number should be large. The residence time $\tau_{residence}$ is defined as:

$$\tau_{residence} = L / V$$

where

$$V = \frac{\dot{m}}{(\pi d_i^{\,2} / 4)}$$

For a micro-combustion tube, the residence time is very small due to high velocity and short length. The chemical time is a function of temperature, higher the temperature, lower the chemical time. In current problem, heat is transferred from outer tube to inner tube and hence reactant temperature is increased resulting in decreased chemical time.

In order to illustrate importance of heat recirculation, consider combustion in micro-tubes under two cases. The first case is tube with heat recirculation, the other is tube with its wall exposed directly to environment. The heat generated by chemical reaction is proportional to the tube volume and heat loss from the tube wall is proportional to the surface area. As the tube diameter decreases, the surface area to volume ratio increases. That means that the heat loss is higher than the heat generation per unit length. As the diameter decreases to a value called quenching diameter, flame cannot be maintained. If

the mixture is very lean or very rich, the quenching diameter is high. Figure 5.6 shows the variation of quenching diameter versus equivalence ratio for methane/air mixture with and without heat recirculation for the base case data.

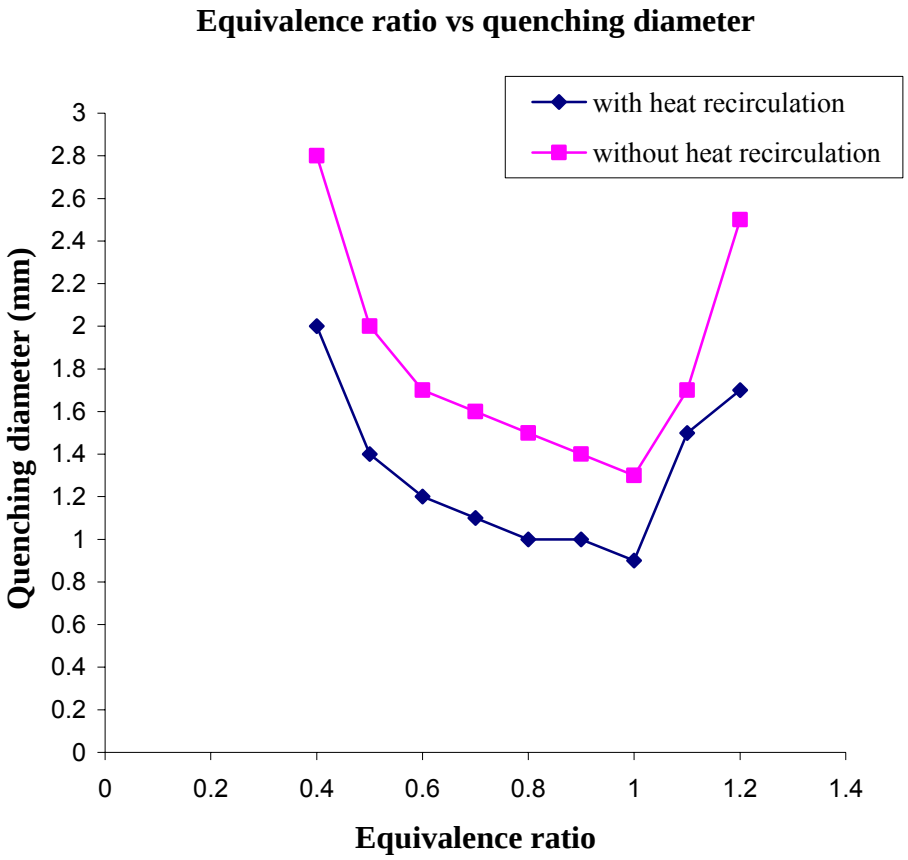

Fig. 5.6 CH4/air quenching diameter at different equivalence ratio (base case)

Similarly, at fixed tube diameter, extremely high or low Reynolds number will also lead to quenching because mixture at low Reynolds number has less amount of heat energy (due to low fuel supply rate) to sustain combustion, and mixture at high Reynolds

number lead to insufficient resident time compared to the chemical reaction time scale. Fig 5.7 shows that Reynolds number as low as 53 can support combustion with heat recirculation. The average inner gas temperature T_{avg} is defined as:

$$T_{avg} = \frac{\sum_{i=1}^{N} T(i)}{N}$$

where, N is nodes number of the inner tube.

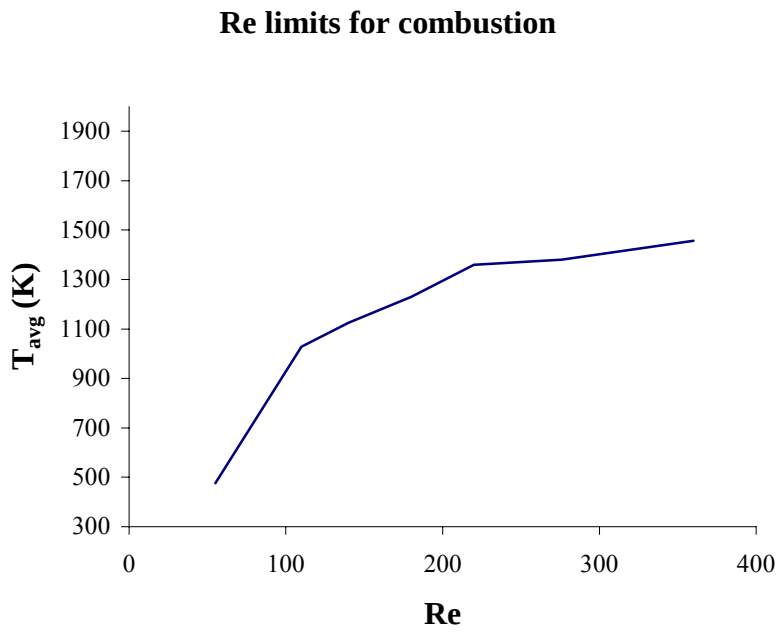

Fig. 5.7 Average gas temperature in the inner tube at dia =2 mm

The quenching distance for CH_4/air is 3.3 mm at standard air conditions without heat recirculation. Heat recirculation will help to obtain combustion in micro-combustor with diameters smaller than 3.3 mm. The calculations indicate that for stoichiometric

premixed CH_4/air combustion in combustor with heat recirculation, the diameter can be as small as 0.5~1 mm.

5.5 Effect of mixture inlet velocity on quenching diameter and LFL

For a micro-TPV system, increased fuel inlet temperature will produce increased power output, but a very high inlet velocity requires larger diameter of tube. The quenching diameter was obtained by keeping velocity fixed and decreasing inner diameter below certain value called quenching diameter where no stable solution can be obtained. As velocity is increased, more fuel is burnt and more energy input is available to the combustor. Beyond certain velocity, the flame is pushed toward the end of inner tube due to decreased residence time and hence decreased chemical heat release make quenching diameter increase. Figure 5.8 illustrates the relationship between fuel inlet velocity and quenching diameter.

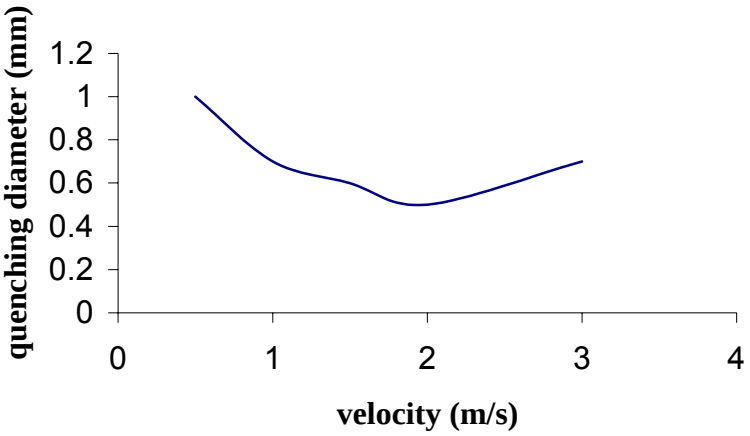

Fig. 5.8 Quenching diameter at different inlet velocity

Figure 5.9 illustrates the effect of fuel inlet velocity on ϕ at lean limit.

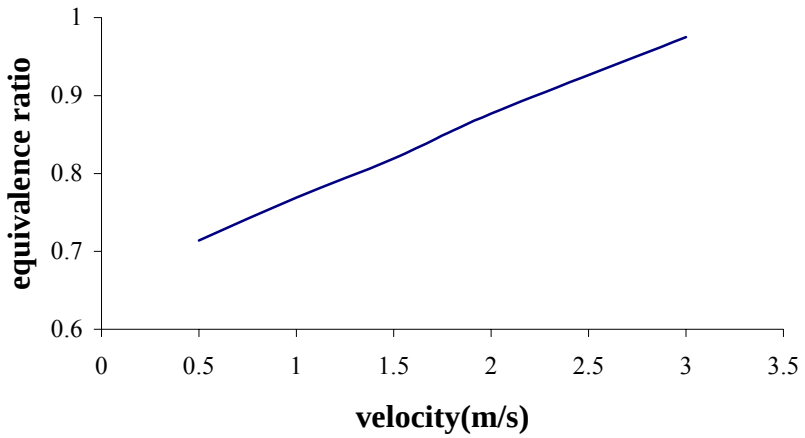

Fig. 5.9 Equivalence ratio at LFL for different fuel inlet velocity

5.6 Effect of heat transfer coefficient

Heat transfer coefficient is a very important factor which would influence the effect of heat recirculation and overall energy conversion efficiency of the TPV system. The estimation of heat transfer coefficient is very coarse in the current model. Further the heat transfer coefficient could be augmented if wall was grooved or made of rough walls. Hence a parametric study was conducted on heat transfer coefficient which is artificially altered in this study in order to study its effect.

Figure 5.10 illustrates the tube exit gas temperature and average outer wall temperature at different heat transfer coefficients. According to the assumptions, the heat transfer coefficients in the inner tube and outer tube are set to be equal.

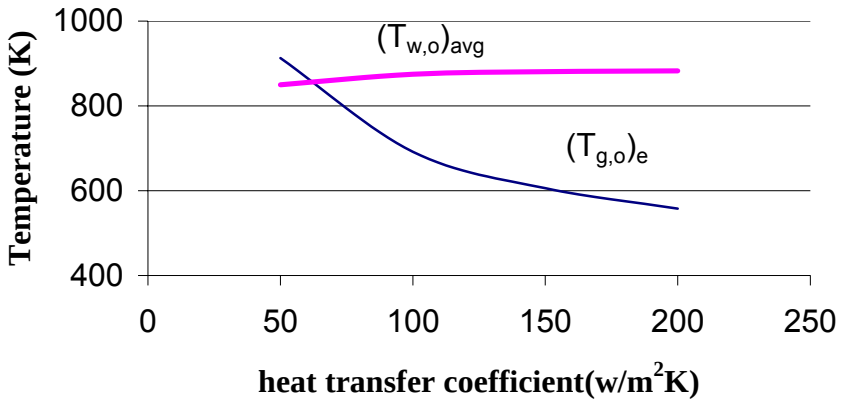

Fig. 5.10 Effect of heat transfer coefficient on exit gas temperature $(T_{g,o})_e$ and average wall temperature of the outer tube $(T_{w,o})_{avg}$

Figure 5.11 illustrates overall energy conversion efficiency η_{con} and heat recirculation efficiency η_{rec} according to variable heat transfer coefficient. The heat recirculation efficiency is defined as following:

$$\eta_{rec} = \frac{heat\ recirculated}{chemical\ heat\ input} = \frac{\int h_H \pi D_i (T_{out}(x) - T_{in}(x)) dx}{\rho u h_c Y_{F,0}}$$

The heat transfer from the gas in outer tube to the gas in inner tube is estimated along the tube when $T_{g,o}$ in the outer tube is higher than $T_{g,i}$ in the inner tube.

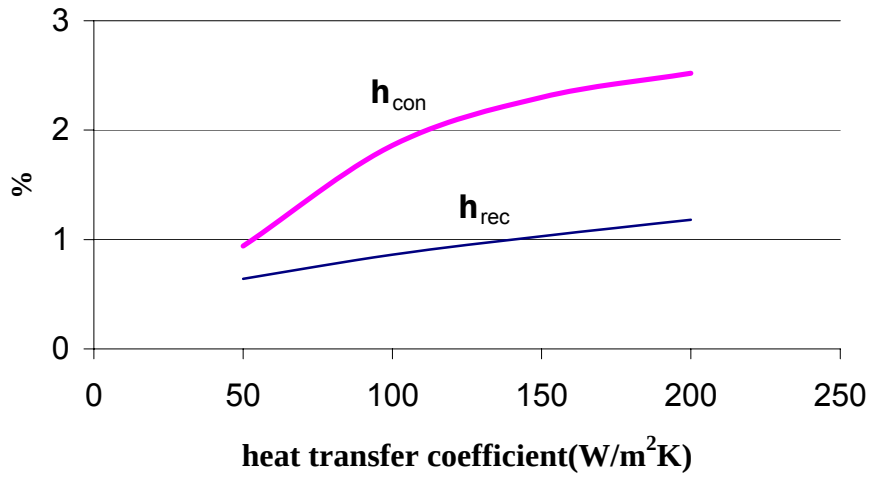

Fig. 5.11 Effect of heat transfer coefficient on heat recirculation efficiency η_{rec} and overall energy conversion efficiency η_{con}

.

From the figure, we can see that higher heat transfer coefficients lead to better heat recirculation. We can enhance the heat transfer by increasing heat transfer coefficient and then get a broader flame flammability and smaller quenching diameter.

5.7 Radiation heat loss

5.7.1 Effect of characteristic size

The energy input is proportional to D^2 at constant velocity while the radiation heat loss is proportional to d. Hence radiation heat loss to energy input ratio is increased as tube diameter is decreased since energy input decreases at faster rate. Thus radiant heat input to TPV cells is decreased which will decrease net electrical power output as micro-combustor size is decreased. Combined with the increased view factor, the radiation heat loss becomes very important for micro-scale tube.

Fig. 5.12 illustrate the surface area to volume ratio φ_1

$$\varphi_1 = \frac{surface\ area}{volume} = \frac{S}{V} = \frac{\pi d_i L}{1/4\,\pi d_i^{\,2} L} = \frac{4}{d_i} \qquad (\frac{1}{mm}) \tag{5-1}$$

Fig. 5.12 also illustrates the effect d_i on surface radiation heat loss fraction φ_2 which is defined as a ration of the surface heat loss to total energy input.

$$\varphi_2 = \frac{E_{radiation}}{E_{in}} = \frac{\varepsilon C \Delta x \sum_{i=1}^{n} \left\{ \int_0^{\infty} \frac{C_1 \lambda^{-5}}{e^{C_2/[\lambda T(i)]} - 1} d\lambda \right\}}{\rho u A_i h_c} \tag{5-2}$$

where N denotes the nodes number of outer tube.

The calculation is based on the base case data. From the figure, it is seen that with the decrease of characteristic size d_i, radiation heat loss from wall surface increases

dramatically. However, small characteristic size has an advantage in components that use heat transfer in their operation such as TPV system.

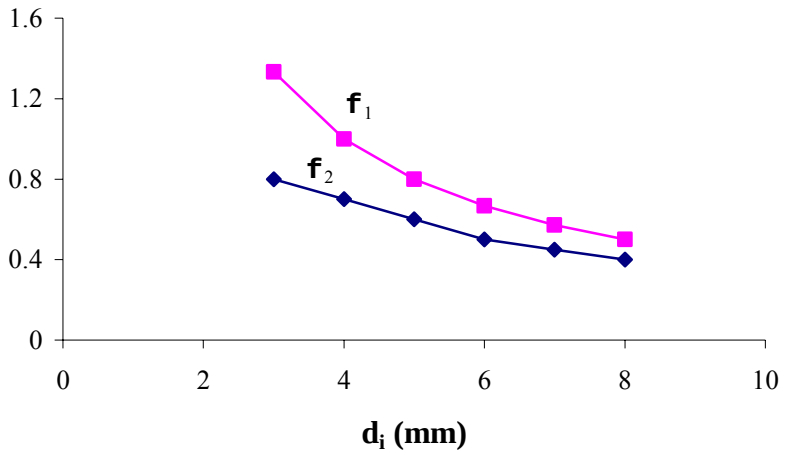

Fig. 5.12 Surface area to volume ratio φ_1 and radiation heat loss fraction φ_2 of micro-combustors

5.7.2 Radiation heat loss along the outer tube

Fig. 5.13 shows the variation of outer wall temperature $T_{w,o}$, heat radiation $\dot{Q}''_{rad}$ and heat absorbed $\dot{Q}''_{abs}$ by photovoltaic cells. It was mentioned earlier that radiation energy with $\lambda < 1.7\mu m$ is absorbed by GaSb cells. Planck's radiation law was used in determine the fraction of energy absorbed by TPV cells. Also, it is seen that higher the wall temperature $T_{w,o}$, higher the amount radiated.

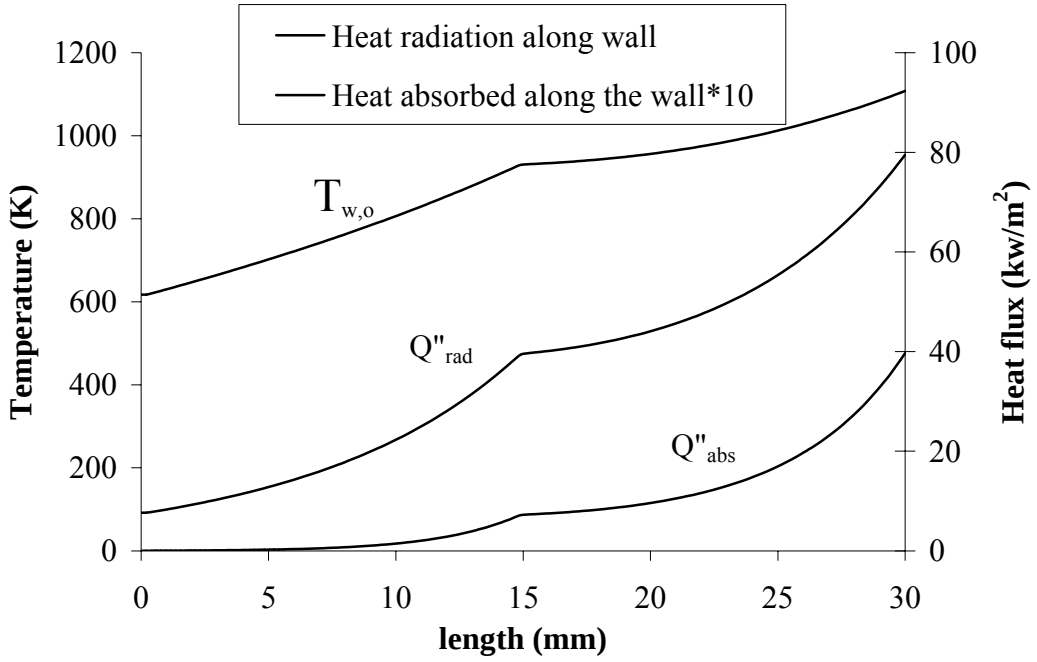

Fig. 5.13 Outer wall temperature and radiation flux distribution for the outer tube

5.8 Direct energy conversion

The conversion of thermal energy into electrical energy is achieved by thermophotovoltaic cell which covers the outer surface of micro-combustor to absorb the heat radiated.

Fig. 5.14 shows the effect of tube diameter on the overall energy conversion efficiency with 1 m/s inlet velocity of stoichometric mixture.

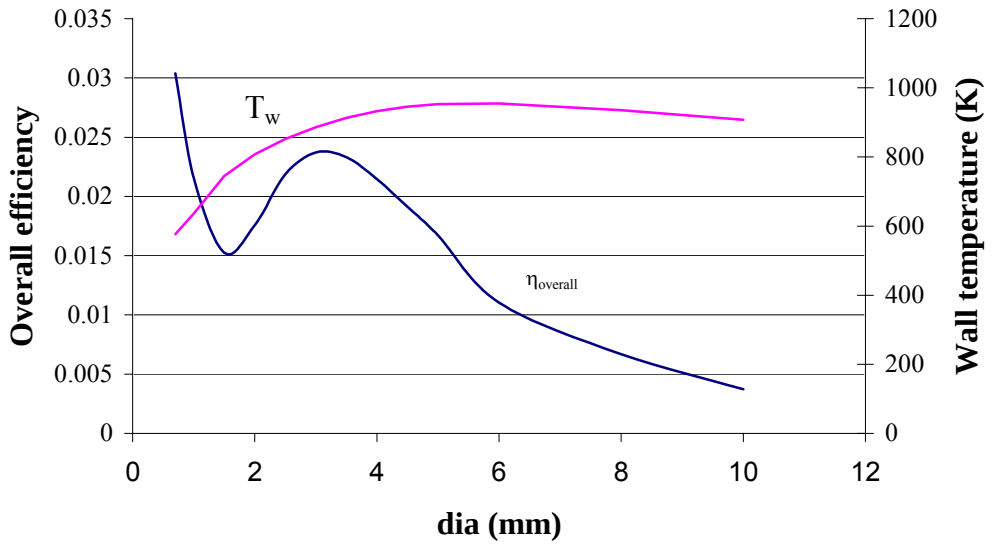

Fig. 5.14 Energy conversion efficiency vs combustor diameter

For example, for a micro-tube with inner diameter 2mm,

The radiation efficiency η_{rad} is:

$$\eta_{rad} = Q_{rad} / Q_{fuel} = 0.92$$

The TPV conversion efficiency η_{TPV} is:

$$\eta_{TPV} = Q_{electic} / Q_{rad} = 0.019$$

The overall efficiency $\eta_{overall}$ is:

$$\eta_{overall} = \eta_{rad} \times \eta_{TPV} = 0.0175$$

Both the wall temperature and surface area to volume ratio will influence the heat radiation as well as the over all energy conversion efficiency. From the figure, the wall temperature drops with inner diameter drops from 1.5 mm, but the surface area to volume ratio dominates the heat radiation, so the overall efficiency increase with the decrease of inner diameter. In the section of 1.5 mm to 3 mm, the wall temperature dominates the heat radiation, so the overall efficiency increases with the increase of inner diameter. For the diameters bigger than 3 mm, the change of outer wall temperature become smooth and the surface area to volume ratio dominates the heat radiation again.

6. SUMMARY AND FUTURE WORK

6.1 Summary

A theoretical model was developed and used to simulate the combustion and direct energy conversion in a micro-combustor.

For a fixed tube diameter such as 3 mm, the maximum heat input is 70w; otherwise the flame is blown off.

In a micro-TPV system, the relative high radiation heat loss has a positive effect on the energy conversion because the thermal photovoltaic cell will absorb heat radiation for energy conversion. The energy conversion efficiency increases as diameter decreases from 1.5mm.

The experiments of Fu [5] confirm the current theoretic model very well. Thus, it is inferred that combustion in a MEMS scale combustor can be achieved by reducing heat losses from the system. The flame can be established in micro-combustor even at a very small Reynolds n/umber (Re=53, energy input is 10W) with heat recirculation.

The flammability range decreases when diameter of combustor decreases. But with heat recirculation, flammability range has been broadened comparing to the flammability limits of methane/air mixture without heat recirculation.

The energy converse efficiency increases dramatically when the diameter decreases from 1.5 mm to 0.5 mm. The energy conversion efficiency will also be influenced by gas flow Reynolds number.

Both experiments and theoretical simulations have proved the feasibility of the combustion in micro-scale and its application to micro-energy devices.

In this micro-combustion model, one can achieve a power output 2.37 Watt with overall efficiency 5.45% for a micro-tube with 3 mm inner diameter and 30 mm length.

6.2 Future work

Establish 2-D combustion and heat transfer model by accounting for radial temperature gradient.

Because the research in this field is still in its early stage, this study provides only theoretical simulation of combustion in a micro-scale and compares with the results achieved previously by the other peer. In the future, experiments must be conducted to get experimental validation.

Catalytic effects must be included in the combustion, such as micro-tube with diameter smaller than 1mm. Catalytic combustion can help to improve micro-combustion performances.

One should study the effect of admitting combustible mixture in the outer tube and exhaust through inner tube.

Study the influence of fuel and oxygen concentration gradients on the combustion performance.

REFERENCES

[1] Khanna R 2003 MEMS fabrication perspectives from the MIT microengine project *Surface and Coatings Technology* **163** 273-280

[2] Pello A 2002 Micropower generation using combustion: issues and approaches *Proceeding of the Combustion Institute* **29** 883-899

[3] Epstein A H, Senturia S D, Anathasuresh G, Ayon A, Breuer K, et al. 1997 Power MEMS and microengines *Proc. IEEE Transducers '97 conf.* (*Chicago*) 753-756

[4] Fu K, Knobloch A, Martinez F, Walther D, Fernandez-Pello A C, et al. 2001 Design and experimental results of small-scale rotary engines *Proc. 2001 ASME International Mechanical Engineering Congress and Exposition* IMECE2001/MEMS-23924

[5] Fu K, Knobloch A, Cooley B, Walther D, Liepmann D, et al. MicroScale combustion research for applications to MEMS rotary IC engine 2001 *Proc. ASME NHTC'01, 35th National Heat Transfer Conf.* NHTC2001-20089

[6] Epstein A H 2003 Millimeter-scale, MEMS gas turbine engines *Proc. ASME Turbo Expo 2003, Power for Land, Sea and Air* GT-2003-38866

[7] Chou S K 2004 Development of a novel micro thermophotovoltaic power generator http://www.eng.nus.edu.sg/EResnews/0310/rd/rd_4.html

[8] Yang W M et al. 2003 Microscale combustion research for application to micro thermophotovoltaic systems *Energy Conversion and Management* **44** 2625-2634

[9] Yang W M, Chou S K, Shu C, Li Z W, Xue H 2002 Combustion in micro-cylindrical combustors with and without a backward facing step *Applied Thermal Engineering* **22** 1777-1787

[10] Sitzki L, Borer K, Schuster E, Ronney P D 2001 Combustion in microscale heat-recirculating burners *The Third Asia-Pacific Conference on Combustion* (*Seoul*)

[11] Desoete G 1967 Stability and propagation of combustion waves in inert porous media *11th Symposium (International) on Combustion* (*Pittsburg*) 959-966

[12] Lee D H, Kwon S 2002 Heat transfer and quenching analysis of combustion in a micro combustion vessel *Journal of Micromechanics and Microengineering* **12** 670-676

[13] Karniadakis G E, Beskok A 2002 *Micro Flows: Fundamentals and Simulation* (New York: Springer)

[14] Borman G L, Ragland K W 1998 *Combustion Engineering* (Boston: McGraw-Hill)

[15] Lewis B, von Elbe G 1987 *Combustion, Flames and Explosions of Gases* 3rd edn (New York: Academic Press)

[16] Cengel Y A, Turner R H 2001 *Fundamentals of Thermal-Fluid Sciences* (Boston: McGraw-Hill)

[17] Rohsenow W M, Hartnett J P, Cho Y I 1998 *Handbook of Heat Transfer* 3rd Edn (New York: McGraw-Hill)

[18] Incropera F P, DeWitt D P 1996 *Fundamentals of Heat and Mass Transfer* 4th edn (New York: John Wiley and Sons)

[19] Partankar S V 1980 *Numerical Heat Transfer and Fluid Flow* (Washington: Hemisphere Pub. Corp.)

[20] Tao W 1998 *Numerical Heat Transfer* (Xi'an, China: Xi'an Jiaotong University Publishing House)

[21] Bartok W, Sarofim A F 1991 *Fossil Fuel Combustion: A Source Book* (New York: John Wiley & Sons)

[22] Annamalai K, Puri I 2005 *Combustion Science and Engineering* (Boca Raton: CRC Press) forthcoming

APPENDIX A

ENERGY BALANCE VALIDATION AND SPICIFIC ENERGY OF TPV SYSTEM

The conditions for the base case are given as:

$u = 1\ m/s$

$\phi = 0.83$

$y_F = 0.046$

$d_i = 3\ mm$

$d_o = 3\ mm$

$L = 30\ mm$

$T_{in} = 300\ K$

$T_\infty = 300\ K$

$P = 1\ bar$

$h_c = 50,000\ kJ/kg$

$M = 28\ kg/kmole$

$c_p = 1.4\ kJ/kg \cdot K$

The outer wall temperature shows in the following figure:

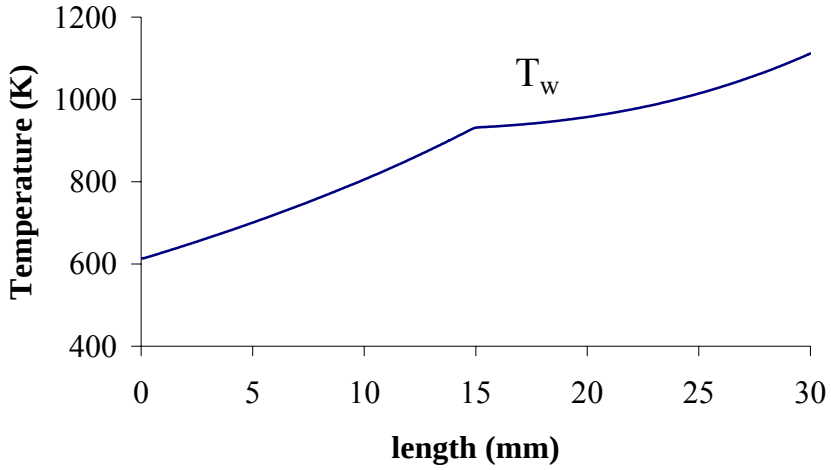

Fig. A.1 Outer wall temperature profile

a) The input energy $\dot{Q}_{in}$ is calculated as:

$$\begin{aligned}\dot{Q}_{in} &= \dot{m} \times y_F \times h_c \\ &= \frac{P}{RT_{in}} u \frac{\pi d_i^{\,2}}{4} \times M \times 0.046 \times 50000 \\ &= 2.862 \times 10^{-7} \times 28 \times 0.046 \times 50000 \\ &= 18.43\ w\end{aligned}$$

b) The calculated radiation energy of the outer tube $\dot{Q}_{rad}$ using combustion code is:

$$\dot{Q}_{rad} = \varepsilon \sigma \int_0^L \left[T(x)^4 - T_\infty^{\,4} \right] \pi d_o dx = 14.25\ w$$

$$\frac{\dot{Q}_{elec}}{\dot{m}_{fuel}} = \frac{14.25 \times 10^{-3}}{2.862 \times 10^{-7} \times 28 \times 0.046} = 38656\ \frac{kJ}{kg}$$

c) The outlet gas temperature T_{out} calculated from the combustion code is:

$$T_{out} = 688.5\ K$$

The exhausted energy $\dot{Q}_{out}$ is:

$$\begin{aligned}\dot{Q}_{out} &= flowrate \times M \times c_p \times (T_{out} - T_{in}) \\ &= 2.867 \times 10^{-7} \times 28 \times 1.4 \times (688.5 - 300) \\ &= 4.37\ w\end{aligned}$$

d) From the energy balance, the calculated error *err* is:

$$err = \left| \frac{\dot{Q}_{in} - \dot{Q}_{rad} - \dot{Q}_{out}}{\dot{Q}_{in}} \right| \times 100\% = \left| \frac{18.43 - 14.25 - 4.37}{18.43} \right| \times 100\% = 1.03\%$$

APPENDIX B

THE CHANGE OF GAS TEMPERATURE PROFILE DURING THE IGNITION AND COMBUSTION PROCESSES

In order to study the effect of initial profile assumptions on the final ignition location, the following two cases were studied based on the base case inlet conditions:

Case (I): For the kinetics of oxidation, the activation energy of methane/air reaction, E=202408 kJ/k mole. Figure B.1 illustrate the temperature profiles of gas in the inner tube for iteration numbers K=0, 1, 2, 3, and 17. At K=0, a direct delta function type profile was assumed with T = 300 K for all locations except at location X = 15 mm where T was assumed to be T=2500 K. Thus a priori assumption is made that ignition occurs at X=15 mm for K=0. The step size selected for iteration is ΔX= 0.96 mm. Convergence occurred after 17 iterations. For this case, the final ignition location is same as location as assumed initially.

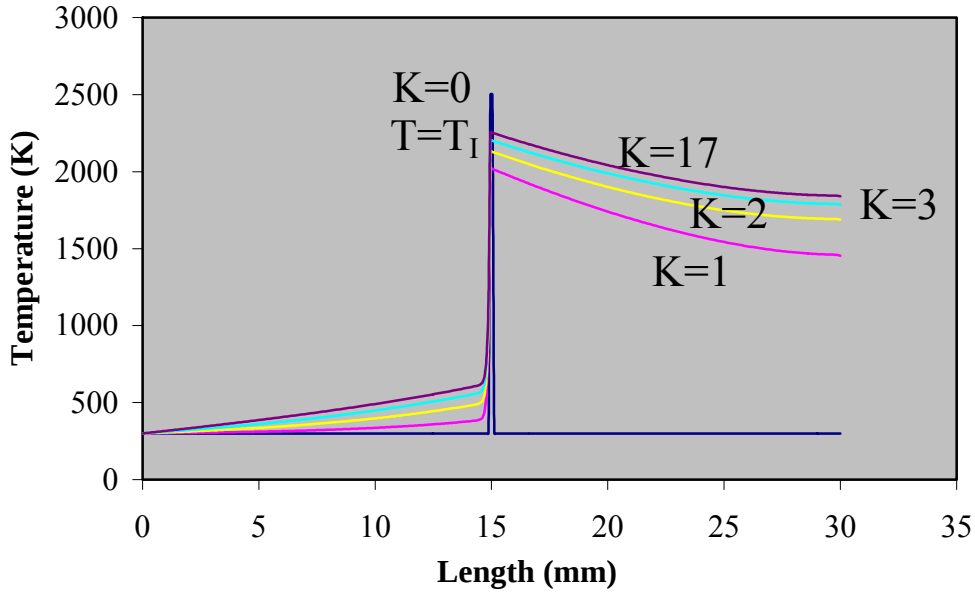

Fig. B.1 Temperature profile development with iteration number for E=202408 kJ/kmole

The effects of starting with different ignition locations in the initial temperature profiles were studied. Figure B.2 gives the converged steady state gas temperature profiles in the inner and outer tube according to different ignition location X. It appears that the converged solution for ignition location is same as the assumed location. When we start ignition with earlier location (X=7.5 mm), the gases in the inner tube transfer heat to outer tube and hence temperature starts decreasing after complete combustion for 7.5 mm<X< 30 mm. However the gases in the outer tube start with a lower temperature at X= 30 mm, it gains heat from inner tube but looses more via radiation to the thermo-voltaic cells. Thus the gas temperature starts decreasing from X= 30 mm to X= 7.5mm. However when X< 7.5 mm, the inner tube temperature is very low and hence it

transfers heat to inner tube and as well looses heat via radiation. Once the inner gas temperature reaches around 800 K, it ignites.

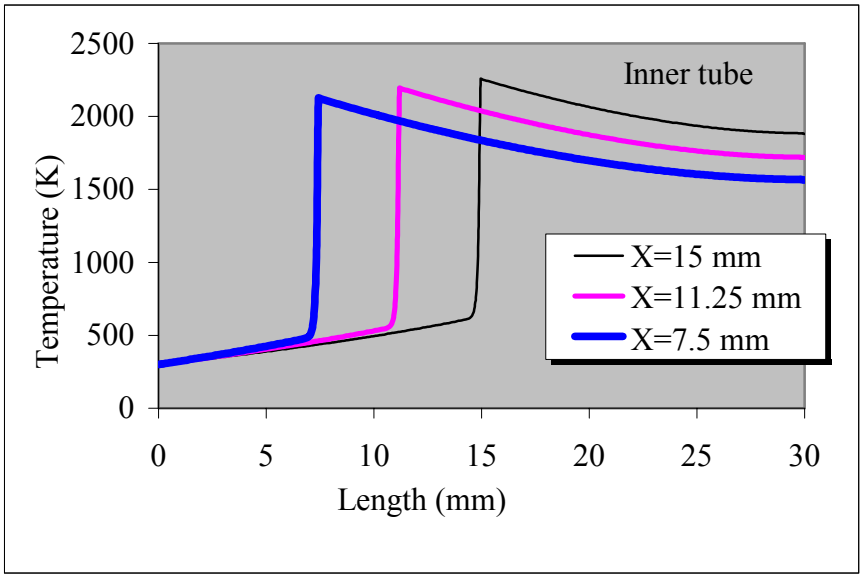

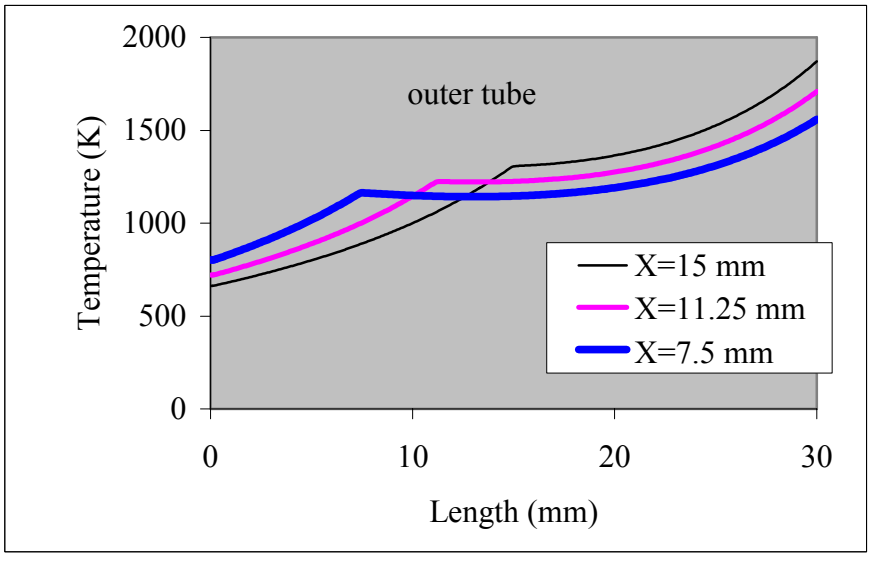

Fig. B.2 Inner and outer wall temperature profiles for E=202408 kJ/kmole

Case (II) The activation energy was reduced by half; thus E changed from 202408 to 101204 kJ/ kmole. Step size was kept same. Figure B.3 illustrates the temperature profiles for case (II) for the same initial profile as assumed in Case (I). It is seen that the ignition location shifted from X= 15 mm (assumed as starting location) to X= 5mm after convergence.

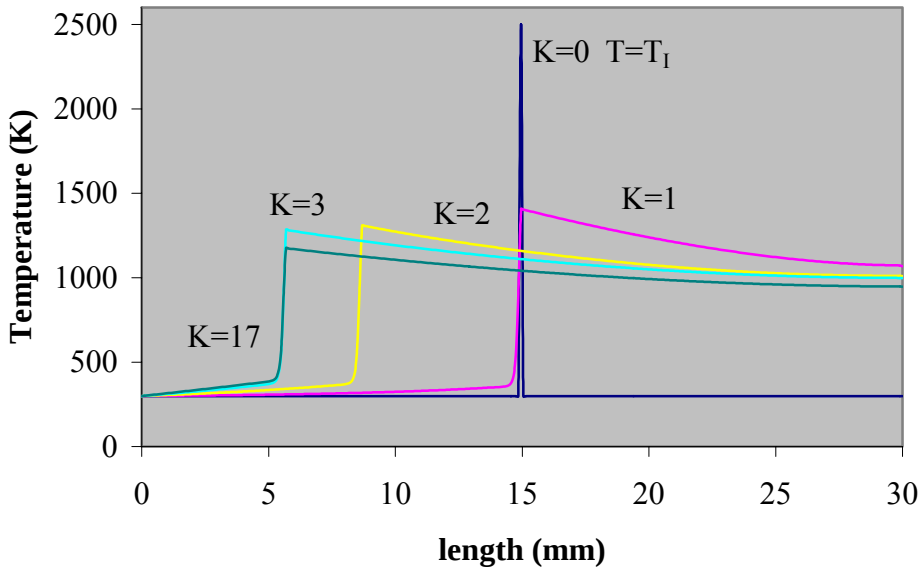

Fig. B.3 Temperature profile development with iteration number for E=101204 kJ/ kmole

The effects of starting with different ignition locations in the initial temperature profiles were studied for case (II) also. Figure B.4 gives the converged steady state gas temperature profiles in the inner and outer tube according to different ignition location X. It appears that the converged solution for ignition location is now different compared to

the assumed location. All starting ignition locations seem to converge at 7.5 mm. As opposed to changing T profiles due to different ignition locations, here the converged T profiles in both inner and outer tubes do not change since the converged ignition location did not change.

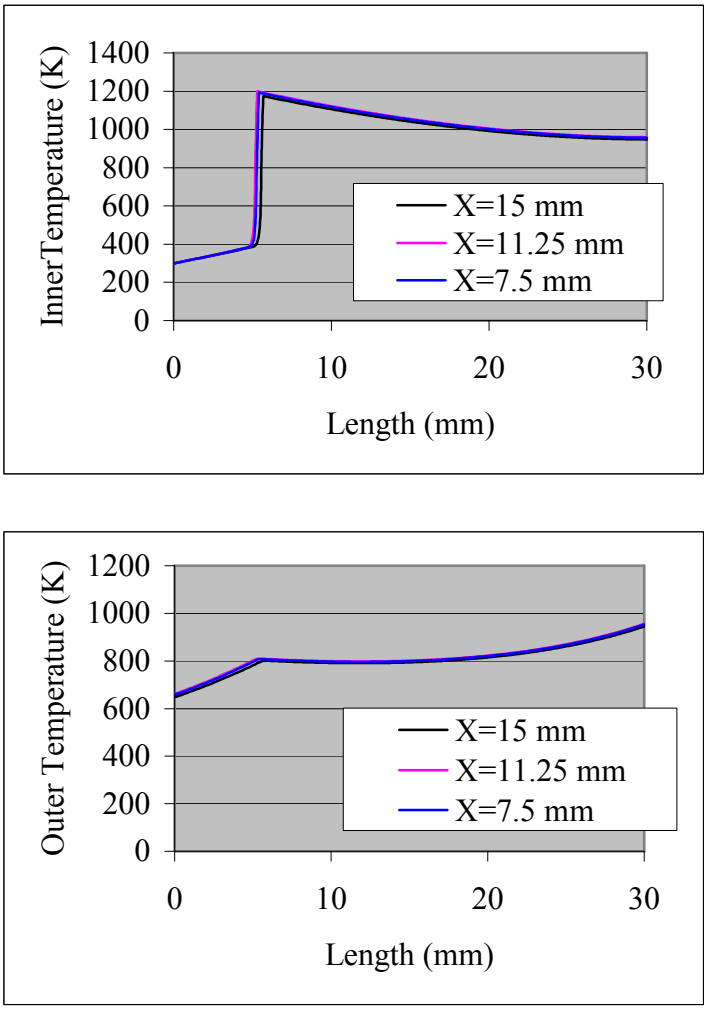

Fig. B.4 Inner and outer wall temperature profiles for E= 101204 kJ/kmole

APPENDIX C

APPROXIMATE SOLUTION FOR IGNITION LOCATION

The ignition location of micro-combustor can be calculated using energy balance. For the base case, for example, the general conditions are given as the following:

Length=0.03 m

d=3 mm

$\dot{m} = 8.01\times10^{-6}$ kg/s

Cp=1.4 kJ/kgK

T_{ign}=850 K

T_{in}=300 K

h = 0.055 kW/m^2 K

If the inlet gas is to be preheated to the ignition temperature 850K, the total energy need is: $Q_{need}=mCp\ (T_{ign}-T_1) =6.168x10^{-3}$ kW

The total heat recirculation is given as:

$$Q_{recir}= h\pi D\ X_{Ign}\ (\bar{T}_{out} - \bar{T}_{in}) \approx h\pi D\ X_{ign}\ (T_{out}-T_{in}),$$

Where, X_{ign} is the length from inlet (outlet) to ignition location. $\bar{T}_{out}$ is the average temperature of the gas in the outer tube between ignition location and outlet. $\bar{T}_{in}$ is the average temperature of the gas in the inner tube between ignition location and inlet.

$T_{out} \approx 660$ K, T_{in}=300 K

Let $Q_{need}=Q_{recir}$, then one obtains X_{ign} =30 mm which is the total combustor length. Note that Q_{cond} is neglected here, because it is very small.

One can try to make the combustor longer, but longer combustor means more heat radiation from the outer tube and less heat recirculation from outer tube to inner tube. In this case, the amount of heat recirculation is not enough to be the only resource for fuel ignition.

When the activation energy is reduced by half, E is reduced from 202408 to 101204 kJ/ kmole. For this case, X_{ign}/L =0.15 assuming T_{ign} =500 K. This result is approximately the same as the value from numerical code which is about 0.17.

APPENDIX D

MICRO-COMBUSTION CODE

```
program Micro-combustion
DOUBLE PRECISION::Cp,LAMDA,DX,Hc,Hc1,LENGTH,T_in,DELT_T,VOL,
Ac,EXCESS,P,AA,ALPHA,BETA,N1,N2,E,R,dt,FUELFLOWRATE,
OXYGENFLOWRATE,X_FUEL,
X_O2,M,M_FUEL,M_O2,T_ign,T_ini,F1,F2,Rito,EM,SB,TW,TW1,
FLOWRATE,F3,F4,Pe,DIA1,DIA2,HA1,HA2,C1,C2,T_SURR,Rt1,Rt2,Rt3,
MASSFLOWRATE,LAMDA1,LAMDA2,LAMDA3,Eb,E_absorb,E_totalabsorb,
E_fuel,CONST1,CONST2,Eff1,Eff2,FUELFLOWRATE1,VISCOSITY,Re,X,
T1,T2,T3,Nu,LEN,Pr,PHI
INTEGER:: N,I,J,K,L,II
DOUBLE PRECISION,DIMENSION(10001)::V,T,B,W,WW,K1,K2,K3,K4,RHO,YF,
     YO2,C_FUEL,C_O2,T0,ATP,ATW,ATE,SOURCE,T_WALL,T_WALL1,C
DOUBLE PRECISION,DIMENSION(10001,3)::A
DOUBLE PRECISION,DIMENSION(10000) :: Qx,Qy,Q,E_rad,E_abs
OPEN(1,FILE="RESULT.DAT")
EXCESS=0.2
PHI=1/(1+EXCESS)
M=28
M_FUEL=16
M_O2=32
V(1)=1 ! M/S
Cp=1.4    ! KJ/KG.K
LAMDA=0.0763E-3 ! KW/M.K
VISCOSITY=17E-6  !KG/M.S
Pr=0.56         !FLUE GAS
Hc=800000   ! KJ/KMOLE   CH4 as fuel
Hc1=50000   ! KJ/KG      CH4 as fuel
LENGTH=0.06    ! METER
LEN=LENGTH/2
DIA1=0.003 !m
DIA2=(2*DIA1**2)**0.5  ! m  outter diameter of outter tube
Ac=3.1416*DIA1**2/4.
C1=3.1416*DIA1
C2=3.1416*DIA2

T_in=300
T_ign=850
T_SURR=300

R=8.314          ! KJ/(KMOLE K)
P=101            ! KPa

RHO(1)=P*M/(R*T_in)
Pe=2.0
DX=Pe*LAMDA/(RHO(1)*V(1)*Cp)
N=INT(LENGTH/(2*DX))
Re=RHO(1)*V(1)*DIA1/VISCOSITY
```

```
Nu=4.364
HA2=Nu*(LAMDA/DIA1)
HA1=HA2/2

VOL=Ac*DX
dt=DX/V(1)          ! S (SECOND)
AA=1.3*1E+9
N1=0.
N2=0.
ALPHA=-0.3
BETA=1.3
E=202408     ! KJ/KMOLE
X_FUEL=1/(1+2*(1+EXCESS)*(1+3.76))
X_O2=2*(1+EXCESS)*X_FUEL
FLOWRATE=P/(R*T_in)*V(1)*Ac !   KMOLE/S
MASSFLOWRATE=FLOWRATE*M   !  KG/S
FUELFLOWRATE1=FLOWRATE*X_FUEL*M_FUEL  !   KG/S

DO I=N+1,2*N
T_WALL(I)=300
END DO

DO I=1,2*N
T(I)=T_in
T0(I)=T_in
END DO

DO WHILE(Rt3>=0.01 .OR. L==0)
L=L+1
J=0
DO WHILE(Rt1>=0.00001 .OR. J==0)
J=J+1

DO I=2,2*N
V(I)=(T(I)/T(I-1))*V(I-1)
END DO

DO I=1,2*N
C(I)=P/(R*T(I))
RHO(I)=C(I)*M
K1(I)=LAMDA/(RHO(I)*V(I)*Cp)
K2(I)=HA1*C1/(RHO(I)*V(I)*Cp*Ac)
K4(I)=HA2*C2/(RHO(I)*V(I)*Cp*Ac)
END DO

IF(L==1 .AND. J==1)THEN
I=INT(N/2)
T(I)=2500
END IF

DO I=1,2*N
K3(I)=0
W(I)=0
```

```
END DO

FUELFLOWRATE=FLOWRATE*X_FUEL*M_FUEL  !    KG/S
OXYGENFLOWRATE=FLOWRATE*X_O2*M_O2

I=0
K=0
DO WHILE(K==0.AND.I<2*N)
I=I+1
C_FUEL(I)=X_FUEL*C(I)
C_O2(I)=X_O2*C(I)
YF(I)=(C_FUEL(I)/C(I))*(M_FUEL/M)
YO2(I)=(C_O2(I)/C(I))*(M_O2/M)
IF(T(I)>=T_ign) THEN
K=I
END IF
END DO

DO WHILE(YF(K)>=0.0001 .AND. YO2(K)>=0.0001 .AND.
&         T(K)>=T_ign .AND. K<=2*N .AND. K/=0)
W(K)=-1*AA*(T(K)**N1)*(P**N2)*EXP(-1*E/(R*T(K)))
&     *(C_FUEL(K)**ALPHA)*(C_O2(K)**BETA)        ! Kmole/m3.s
C_FUEL(K+1)=(C_FUEL(K)+W(K)*dt)*T(K)/T(K+1)
C_O2(K+1)=(C_O2(K)+2*W(K)*dt)*T(K)/T(K+1)

YF(K+1)=(C_FUEL(K+1)/C(K+1))*(M_FUEL/M)
YO2(K+1)=(C_O2(K+1)/C(K+1))*(M_O2/M)

IF(EXCESS>=0 .AND. YF(K+1)<=0)THEN
W(K)=-1.0*FLOWRATE*(C_FUEL(K)/C(K))/VOL
END IF
IF(EXCESS<0 .AND. YO2(K+1)<=0) THEN
W(K)=-0.5*FLOWRATE*(C_O2(K)/C(K))/VOL
END IF

K3(K)=ABS(W(K))*Hc/(RHO(K)*V(K)*Cp)

K=K+1
END DO

IF(K<2*N .AND. K/=0)THEN

IF(EXCESS>=0 .AND. YF(K)<=0)THEN
YF(K)=0
YO2(K)=2*ABS(EXCESS)*M_O2/(M_FUEL+2*(1+EXCESS)*(M_O2+3.76*28))
END IF
IF(EXCESS>=0 .AND. C_FUEL(K)<=0)THEN
C_FUEL(K)=0
C_O2(K)=2*ABS(EXCESS)/(1+2*(1+EXCESS)*(1+3.76))*P/(R*T(K))
END IF

IF(EXCESS<0 .AND. YO2(K)<=0)THEN
YO2(K)=0
YF(K)=ABS(EXCESS)*M_FUEL/(M_FUEL+2*(1+EXCESS)*(M_O2+3.76*28))
```

```
END IF
IF(EXCESS<0 .AND. C_O2(K)<=0)THEN
C_O2(K)=0
C_FUEL(K)=ABS(EXCESS)/(1+2*(1+EXCESS)*(1+3.76))*P/(R*T(K))
END IF

DO I=K+1,2*N
YF(I)=YF(K)
YO2(I)=YO2(K)
C_FUEL(I)=C_FUEL(I-1)*T(I-1)/T(I)
C_O2(I)=C_O2(I-1)*T(I-1)/T(I)
END DO
END IF

DO I=2,N
ATW(I)=-K1(I)/DX-1
ATP(I)=2*K1(I)/DX+K2(I)*DX+1
ATE(I)=-K1(I)/DX
SOURCE(I)=K2(I)*DX*T(2*N-I+1)+K3(I)*DX
END DO
DO I=N+1,2*N-1
ATW(I)=-K1(I)/DX-1
ATP(I)=2*K1(I)/DX+K2(I)*DX+K4(I)*DX+1
ATE(I)=-K1(I)/DX
SOURCE(I)=K2(I)*DX*T(2*N-I+1)+K3(I)*DX+K4(I)*DX*T_WALL(I)
END DO
DO I=2,2*N-1
A(I,1)=ATW(I)
A(I,2)=ATP(I)
A(I,3)=ATE(I)
B(I)=SOURCE(I)
END DO
A(1,1)=0
A(1,2)=1
A(1,3)=0
B(1)=T_in
A(2*N-1,2)=A(2*N-1,2)+A(2*N-1,3)
A(2*N-1,3)=0

CALL THOMAS (2*N,A,B)

DO I=1,2*N-1
T(I)=B(I)
END DO
T(2*N)=T(2*N-1)

Rt1=0
DO I=1,2*N
Rt1=Rt1+ABS(T(I)-T0(I))
T0(I)=T(I)
END DO

END DO
```

```
      DO I=N+1,2*N
      T_WALL1(I)=T_WALL(I)
      END DO
      EM=0.93
      SB=5.67E-11  !KW/(M2.K4)

      DO I=N+1,2*N
      T1=T_SURR
      T2=T(I)
      Rt2=100
      DO WHILE(Rt2>=0.001)
      T3=0.5*(T1+T2)
      X=EM*SB/HA2*T3**4.0+T3-(T(I)+EM*SB/HA2*T_SURR**4.0)
      IF(X>=0)THEN
      T2=T3
      ELSE
      T1=T3
      END IF
      RT2=ABS(T1-T2)
      END DO
      T_WALL(I)=T1
      END DO

      Rt3=0
      DO I=N+1,2*N
      Rt3=Rt3+ABS(T_WALL1(I)-T_WALL(I))
      END DO

      PRINT*,L,"Rt3=",Rt3
      END DO

      LAMDA1=1.7E-8   !M
      LAMDA2=1.7E-6  !M
      DO I=N+1,2*N
      CALL INTEGRATION_OF_PLANCK_LAW (LAMDA1,LAMDA2,I,T_WALL,Eb)
      E_absorb=EM*Eb   !KW/M2
      E_totalabsorb=E_totalabsorb+E_absorb*C2*DX  !KW
      END DO

      E_radiation=0
      DO I=N+1,2*N
      E_radiation=E_radiation+EM*SB*(T_WALL(I)**4.0)*C2*DX
      END DO
      E_fuel=FUELFLOWRATE1*Hc1  ! KW

      V_AVG=0
      DO I=1,2*N
      V_AVG=V_AVG+V(I)/(2*N)
      END DO
      P_DROP=(64/Re)*LENGTH*V_AVG**2/(2*9.8*DIA1)

      WRITE(1,5),"NODE","T","W","YF","YO2","C_FUEL","C_O2"
5     FORMAT(1X,A6,A4,A15,5A19)
      DO I=1,2*N
```

```
      WRITE(1,10),I,T(I),W(I),YF(I),YO2(I),C_FUEL(I),C_O2(I)
      END DO
10    FORMAT(1X,I4,F9.2,5E19.10)

      END PROGRAM MICRO-COMBUSTION

      SUBROUTINE THOMAS (N,A,B)
      DOUBLE PRECISION,DIMENSION(10001)::B
      DOUBLE PRECISION,DIMENSION(10001,3)::A
      A(1,3)=-A(1,3)/A(1,2)
      B(1)=B(1)/A(1,2)
      DO I=2,N-1
      A(I,3)=-A(I,3)/(A(I,2)+A(I,1)*A(I-1,3))
      B(I)=(B(I)-A(I,1)*B(I-1))/(A(I,2)+A(I,1)*A(I-1,3))
      END DO
      DO I=N-2,1,-1
      B(I)=A(I,3)*B(I+1)+B(I)
      END DO
      RETURN
      END SUBROUTINE

      SUBROUTINE INTEGRATION_OF_PLANCK_LAW (LAMDA1,LAMDA2,I,T_WALL,Eb)
      DOUBLE PRECISION :: LAMDA1,LAMDA2,LAMDA3,Eb,H,CONST1,CONST2
      DOUBLE PRECISION,DIMENSION(10001)::T_WALL
      CONST1=3.742E-19  !KW.M2
      CONST2=1.4388E-2  !M.K
      J=1000
      H=(LAMDA2-LAMDA1)/J
      DO II=1,J+1
      LAMDA3=LAMDA1+(II-1)*H
      SUBSTITUTE=EXP((CONST2/(LAMDA3*T_WALL(I)))/1000)
      SUBSTITUTE=SUBSTITUTE**1000
      IF(II==1)THEN
      Eb=0.5*H*CONST1*LAMDA3**(-5.)/(SUBSTITUTE-1)
      ELSEIF(II==J+1)THEN
      Eb=Eb+0.5*H*CONST1*LAMDA3**(-5.)/(SUBSTITUTE-1)
      ELSE
      Eb=Eb+H*CONST1*LAMDA3**(-5.)/(SUBSTITUTE-1)
      END IF
      END DO
      RETURN
      END SUBROUTINE
```

VITA

Yafeng Lei was born in Hunan province, China in 1975. He received his Bachelor of Engineering degree in thermal energy engineering in 1997 from Tianjin University and then worked in industry for five years. He enrolled in Texas A&M University in August 2002 and graduated in August 2005 with a Master of Science degree in mechanical engineering.

Yafeng Lei may be reached at Texas A&M University, MS 3123 Department of Mechanical Engineering, College Station, TX, 77843. His email address is: leiyafeng@hotmail.com.